Key Points:
- Large-ensemble simulations are needed to fully characterize coupled extremes in the polar vortex and tropospheric jet in early 2020
- Details of the vortex structure play an important role in promoting either reflection or dissipation of upward propagating waves 1 and/or 2
- Modulation of lowermost stratospheric circulation from above and below facilitates co-evolution of tropospheric and stratospheric extremes

Potential Links Between Tropospheric and Stratospheric Circulation Extremes During Early 2020

Philip Rupp[1] , Sheena Loeffel[2] , Hella Garny[2] , Xiaoyang Chen[3], Joaquim G. Pinto[3] , and Thomas Birner[1]

[1]Meteorological Institute Munich, Ludwig-Maximilians-University, Munich, Germany, [2]Deutsches Zentrum für Luft- und Raumfahrt (DLR), Institut für Physik der Atmosphäre, Oberpfaffenhofen, Germany, [3]Institute of Meteorology and Climate Research, Karlsruhe Institute of Technology, Karlsruhe, Germany

Abstract February-March 2020 was marked by highly anomalous large-scale circulations in the Northern extratropical troposphere and stratosphere. The Atlantic jet reached extreme strength, linked to some of the strongest and most persistent positive values of the Arctic Oscillation index on record, which provided conditions for extreme windstorms hitting Europe. Likewise, the stratospheric polar vortex reached extreme strength that persisted for an unusually long period. Past research indicated that such circulation extremes occurring throughout the troposphere-stratosphere system are dynamically coupled, although the nature of this coupling is still not fully understood and generally difficult to quantify. We employ sets of numerical ensemble simulations to statistically characterize the mutual coupling of the early 2020 extremes. We find the extreme vortex strength to be linked to the reflection of upward propagating planetary waves and the occurrence of this reflection to be sensitive to the details of the vortex structure. Our results show an overall robust coupling between tropospheric and stratospheric anomalies: ensemble members with polar vortex exceeding a certain strength tend to exhibit a stronger tropospheric jet and vice versa. Moreover, members exhibiting a breakdown of the stratospheric circulation (e.g., sudden stratospheric warming) tend to lack periods of persistently enhanced tropospheric circulation. Despite indications for vertical coupling, our simulations underline the role of internal variability within each atmospheric layer. The circulation extremes during early 2020 may be viewed as resulting from a fortuitous alignment of dynamical evolutions within the troposphere and stratosphere, aided by each layer's modification of the other layer's boundary condition.

1. Introduction

The dynamical coupling between the troposphere and stratosphere is an important aspect of the climate system with considerable meteorological implications. The resulting correlation between tropospheric and stratospheric variability (e.g., Thompson & Wallace, 1998) can be of particular importance for weather forecasts beyond about 2 weeks lead time since the dynamics of the two layers mostly evolves on substantially different time scales, typically days within the troposphere and weeks within the stratosphere. A comprehensive understanding of the fundamental principles of troposphere-stratosphere interactions can help to improve the accuracy of weather forecasts and climate projections and to extend the corresponding predictable time ranges (e.g., Baldwin et al., 2003; Scaife et al., 2016; Sigmond et al., 2013; Tripathi et al., 2015).

Troposphere-stratosphere dynamical coupling works both upward via planetary wave forcing of the stratospheric circulation (Charney & Drazin, 1961; Matsuno, 1971) and downward, as established observationally, via tropospheric circulation anomalies following stratospheric extremes (e.g., Baldwin & Dunkerton, 2001; Domeisen & Butler, 2020). A useful way to study stratosphere-troposphere (strat-trop) interactions is to analyze stratospheric circulation extremes and their influence on the troposphere, or vice versa. In principle coupling mechanisms related to extremes might not necessarily behave symmetrically for anomalously weak or strong circulations and thus a corresponding distinction is potentially important (e.g., Domeisen et al., 2020).

Extensive literature has focused on the tropospheric response in the Northern hemisphere (NH) following stratospheric polar vortex breakdowns associated with sudden stratospheric warming (SSW) events (Charlton-Perez et al., 2018; Karpechko et al., 2017; Kautz et al., 2020; Tomassini et al., 2012). Such conditions are often preceded by the occurrence of upward propagating planetary waves leading to anomalous stratospheric warming and a rapid deceleration of stratospheric winds (Baldwin et al., 2021; Matsuno, 1971). Periods with weakened polar vortex are not necessarily associated with a complete breakdown of the stratospheric circulation (i.e., a major

SSW), but may correspond to so-called sudden stratospheric deceleration (SSD) events with weaker but still westerly stratospheric winds (similar to minor SSW events). The downward influence following such events can lead to an equatorward shift of the tropospheric jet stream, associated with negative anomalies of large-scale modes of tropospheric variability like the Northern Annular Mode (NAM), the Arctic Oscillation (AO), and the Northern Atlantic Oscillation (Beerli & Grams, 2019; Domeisen, 2019). These anomalies can further modify the occurrence of tropospheric weather regimes (e.g., Domeisen et al., 2020; Woollings et al., 2010) and increase the likelihood of extreme surface events like cold-spells (e.g., Huang et al., 2021; Kautz et al., 2020; Kolstad et al., 2010; Thompson et al., 2002).

Studies investigating the tropospheric response to a strong polar vortex are comparatively sparse, and thus both the robustness of the downward coupling of strong stratospheric zonal flows and their influence on extended-range predictability is in particular not yet fully understood. Although many authors find the two stratospheric conditions (strong/weak vortex) to generally have a similar but opposite tropospheric response (Baldwin & Dunkerton, 2001; Thompson et al., 2002; Tripathi et al., 2015), certain differences in response could be expected, for example, based on asymmetries in the potential for strat-trop wave coupling during these situations (further discussed in Section 7). Extended periods with a relatively strong stratospheric vortex were shown to be associated with periods in which the tropospheric NAM tends to be anomalously positive (Limpasuvan et al., 2005) and the mid-latitude jet tends to be strong. Periods of the strong tropospheric jet stream are typically characterized by an increased number of intense mid-latitude cyclones (e.g., Pinto et al., 2009). During the winter 2013/2014, for example, a persistently intensified and more zonal tropospheric jet stream contributed to a period of cyclone clustering (Dacre & Pinto, 2020; Mailier et al., 2006) over the British Isles (Matthews et al., 2014; Priestley et al., 2017), leading to enduring wet and windy conditions and widespread floods in this region (Huntingford et al., 2014; Priestley et al., 2017).

The dynamical processes leading to periods with weak or strong stratospheric polar vortex typically involve anomalies in the vertical wave activity flux F_p (vertical component of the Eliassen-Palm flux) and stratospheric conditions are hence strongly coupled to lower stratospheric planetary wave activity (Birner & Albers, 2017; Dunn-Sigouin & Shaw, 2015). A period of anomalously strong upward wave flux is likely associated with a subsequent SSW or SSD event (e.g., Polvani & Waugh, 2004). On the other hand, periods of anomalously weak upward or even downward wave flux, are likely associated with a subsequent strengthening of the polar vortex. Such periods of downward wave flux are often linked to so-called wave reflection events (WRE), where previously upward propagating waves are reflected downward at reflective surfaces in the upper stratosphere. WREs can strongly influence the structure and strength of the Southern polar vortex on both seasonal and daily time scales (Harnik & Lindzen, 2001), and also occur in the Northern hemisphere, predominantly between January to March (Perlwitz & Harnik, 2003). The occurrence of WREs is caused by the formation of reflective surfaces for meridional and vertical wave propagation, which often follows pulses of upward propagating waves and a strong deceleration of upper stratospheric winds (Harnik, 2009; Harnik & Lindzen, 2001; Perlwitz & Harnik, 2003), consistent with associated changes in the curvature of the zonal mean flow and a corresponding modification of the refractive index (see Section 4 below for details). By considering reflective and non-reflective states of the atmosphere, Perlwitz and Harnik (2004) showed that the former is mostly characterized by downward wave coupling for the NH, while the latter is more often characterized by zonal-mean coupling. Dunn-Sigouin and Shaw (2015) found that the tropospheric impacts resulting from stratospheric vortex decelerations associated with strong upward planetary wave fluxes are larger in magnitude than those resulting from periods with strong polar vortex and downward wave reflection.

Although the tropospheric response to anomalously strong or weak stratospheric circulations is robust in composites (averaging over many cases), the variability across individual cases is high. For example, periods of anomalous stratospheric conditions without any apparent tropospheric signal are not uncommon (Baldwin & Dunkerton, 2001; Domeisen & Butler, 2020; Runde et al., 2016). Furthermore, the strength and vertical structure of the lower stratospheric winds can influence the tropospheric flow evolution (e.g., Rupp & Birner, 2021; Wittman et al., 2007) and persistent lower stratospheric anomalies can produce a coherent tropospheric response (e.g., Hitchcock & Simpson, 2014; Karpechko et al., 2017; Runde et al., 2016). The large variability of strat-trop interactions generally complicates the identification of coherent mechanisms for the downward propagation of stratospheric anomalies into the troposphere and allows for a wide range of possible interactions and behaviors (see, e.g., Domeisen et al., 2020; Domeisen & Butler, 2020; Rao et al., 2020). Hence, caution is required when

analyzing specific cases in a deterministic framework. Taguchi (2008) found that the hypotheses of SSWs either preceding or following tropospheric blocking events could not be supported based on a comprehensive statistical analysis of 49 winter periods, although they note that individual cases can show pronounced signs of an apparent coupling. Recently, Kautz et al. (2020) used an ensemble-simulation approach to analyze the early 2018 SSW event and its contribution to the Eurasian cold spell observed during that winter. They attributed an increased likelihood for cold surface temperatures to the SSW but emphasized the lack of a direct causal link. Such probabilistic analyses with large-ensemble simulations are a useful way to quantify the robust signal of stratospheric downward influence, which is often weak compared to the tropospheric internal variability.

The winter period of 2019/20 was one of the most extreme periods ever recorded in terms of tropospheric and stratospheric dynamics. Both the AO index and the stratospheric polar vortex strength showed extreme positive values and anomalous persistence. Various authors have presented evidence for a strong apparent connection between stratospheric and tropospheric anomalies in that winter (Lawrence et al., 2020; Lee et al., 2020). In particular, the occurrence of a WRE has been suggested to support the development of extreme and persistent tropospheric circulation anomalies in general (Shaw & Perlwitz, 2013) and specifically during early 2020 (Lawrence et al., 2020). Moreover, Hardiman et al. (2020) provided evidence that tropospheric internal dynamics have contributed to the development of the persistent tropospheric circulation anomalies of early 2020 and their unusual high predictability.

The present study aims to analyze the potential links between tropospheric and stratospheric extremes in the large scale zonal circulation from January–March 2020, using a combination of re-analysis and large-ensemble approaches. The paper is structured as follows. Section 2 provides an overview of the numerical model and dataset used. Section 3 discusses the evolution of tropospheric and stratospheric circulation on different scales during early 2020. In particular, we identify multiple periods of extreme atmospheric behavior, for example, a pronounced WRE in early February. Hence, in Section 4 we give a detailed description of the dynamics associated with this WRE and analyze its contribution to strengthening the polar vortex in the following weeks. Section 5 then identifies potential indications for two-way strat-trop coupling, including a downward influence of the WRE and the associated strengthened vortex in February. In contrast to the downward influence of stratospheric flow anomalies induced due to a specific stratospheric behavior like the WRE, Section 6 studies the downward coupling of generally anomalous stratospheric circulations observed during late February and early March. Section 7 then discusses the findings of this paper before, in Section 8, we summarize our main conclusions.

2. Model and Data Set

2.1. ICON Ensemble Simulations

We use the comprehensive 'ICOsahedral Nonhydrostatic' (ICON; version 2.5.0) model of the German weather service (DWD) to perform a series of ensemble forecast simulations (for a detailed description of the dynamical core see Zängl et al., 2015). The model uses a triangular grid with roughly 40 km horizontal resolution and 90 terrain-following height levels in the vertical up to a height of 75 km (with about 40 levels in the extratropical troposphere). The output is interpolated onto a 1° regular grid following 52 levels of constant pressure. We integrate the simulations for 50 days; the time step of the dynamical core of the model runs is 1 min, with output given as 6-hourly data (although some figures only show part of the simulated period and most diagnostics are shown as daily means for easier interpretation).

All simulations are initialized with realistic atmospheric conditions taken from operational ICON analysis products provided by DWD as individual sets of initial conditions for a 40 member ensemble (with slightly perturbed initial conditions for a given initialization date). In order to increase the ensemble size, and thus obtain more robust statistics, we combine several ensembles runs of slightly varying initialization time (with time difference of 1–3 days) to form 'time lagged ensembles'. This approach was first proposed as a method to increase the efficiency of the operational forecast by Hoffman and Kalnay (1983). It has been shown that time lagged ensembles can provide an increased prediction skill for the ensemble mean (likely due to the increase in ensemble size) for medium range forecasts (e.g., Branković et al., 1990; Dalchér et al., 1988). However, we do not primarily intend to use the lagged ensemble approach to improve ensemble mean evolution. Instead, the small temporal offset of the different ensembles is taken to be equivalent to small perturbations of the initial conditions, with the intention of improving the sampling of the underlying probability distribution of possible atmospheric states in the

probabilistic period of the model simulation. A similar approach has previously been used by other authors in probabilistic studies on different time scales ranging from days to months (e.g., Katsafados et al., 2014; Vogel et al., 2014).

The numerical model used in the present study includes parametrization schemes for non-resolved orographic (Lott & Miller, 1997) and non-orographic (Orr et al., 2010) gravity waves, respectively. Further, sea surface temperatures are initialized with data taken from the analysis products mentioned above and varied in time according to daily increments based on the linear interpolation of a monthly mean climatology.

Throughout the paper, the statistical significance of the difference in means is assessed based on the 95% confidence level of a one-sided two-sample Student's t-test. Clusters in Sections 3–6 are defined using thresholds that result in a trade-off between (a) representing extreme behavior in the resulting clusters and (b) sufficiently large sample sizes for robust statistical assessment.

2.2. ERA5 Re-Analysis Data

The ERA5 re-analysis dataset (Hersbach et al., 2020) of the European Centre for Medium range Weather Forecasts (ECMWF) is used as the representation of atmospheric state and behavior during the winter period of 2019/20 and in a climatological sense, with climatology being calculated as the inter-annual average of the years 2000–2019. The dataset used is given as a direct output of the re-analysis on a $1° \times 1°$ regular horizontal grid following pressure surfaces with the temporal resolution of 6h. To reduce any high frequency variability the climatology has been smoothed using a centered 30-day running mean. Throughout the manuscript, we interpret diagnostics based on re-analysis data as observations and thus the true state of the atmosphere.

3. Description and Predictability of the Extremely Anomalous Periods in Early 2020

3.1. Strategy and Definition of Metrics

We start the analysis of extreme tropospheric and stratospheric behavior during the early months of the year 2020 by providing a general description of the observed evolution of the atmosphere (also see Lawrence et al., 2020; Lee et al., 2020) and how it is represented by the ensemble mean of model simulations with varying initialization date.

When interpreting the ensemble evolution of given model integration, we conceptually distinguish between early forecast times, which are strongly influenced by the initial conditions, and later times, where most of the memory of initial conditions is lost. Correspondingly the nature of predictive skill of an ensemble simulation changes over time, transitioning from the prediction of specific atmospheric features as realized in observations by the majority of ensemble members ("deterministic skill") to the prediction of the probability of certain features to arise in the atmospheric flow situation ("probabilistic skill"). This transition occurs gradually over time, and the time scales for the deterministic prediction range of an ensemble forecast depend on the particular phenomenon of interest - for the dynamical evolution of large scale circulations typical time ranges are several days within the troposphere and a few weeks within the stratosphere.

For most of the following analyses, we focus on two indices to characterize and quantify the large scale zonal circulation of the troposphere and stratosphere, respectively. We define the U_{10}^{60} index as zonally averaged zonal wind at 60° North and 10 hPa. This is an index typically used to determine the strength and zonal symmetry of the stratospheric polar vortex, and also to define SSWs (with $U_{10}^{60} < 0$). We further define the $\tilde{AO}$ index as the difference in the zonal mean geopotential height at 1,000 hPa of the meridional mean between 30 and 50° North and 60–90° North. This definition is motivated by the spatial empirical orthogonal function (EOF) 'loading' pattern of the Arctic Oscillation (AO) index and can be used as a quantitative measure of the strength, position, and zonal symmetry of the tropospheric mid-latitude jet. The precise definition of $\tilde{AO}$ was chosen so that it provides a strong climatological correlation with the conventional EOF-based AO index provided by the National Oceanic and Atmospheric Administration (NOAA). The correlation between the $\tilde{AO}$ index in ERA5 re-analysis data and the AO index in NOAA data is $r \approx 0.8$ for each individual winter between 1980 and 2020. However, in contrast to the conventional AO index, the $\tilde{AO}$ index can be calculated from the available model simulations without the need for a climatological dataset that would be required to perform the EOF analysis.
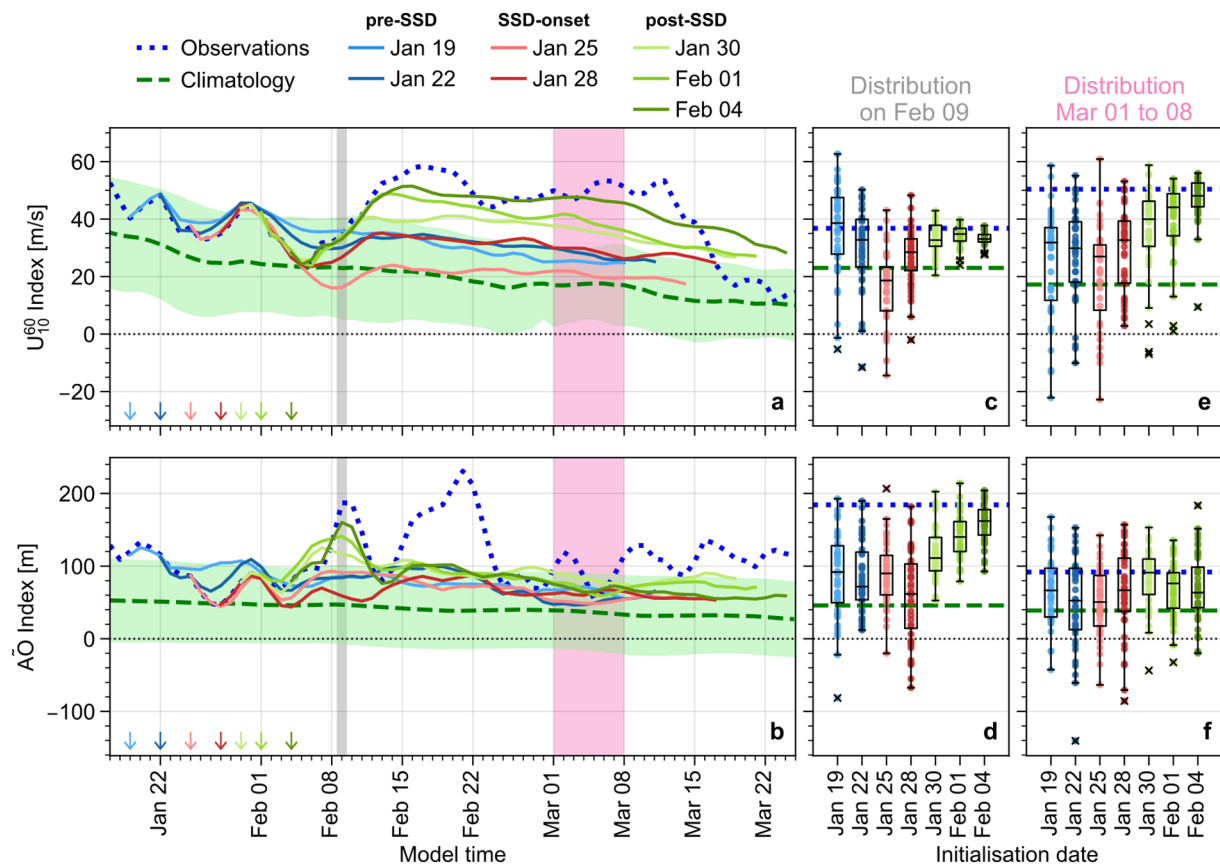
Figure 1. Left column: Evolution of U_{10}^{60} (a) and $\tilde{AO}$ (b) indices in ensemble simulations and re-analysis data. Solid lines: ensemble means for different initialization dates (indicated by arrows on the *x*-axes). Dotted and dashed lines: re-analysis evolution for early 2020 and climatology, respectively, with corresponding shading indicating the climatological variability in terms of one standard deviation. Right columns: member distribution in U_{10}^{60} (top) and $\tilde{AO}$ (bottom) on February 9th (c) and (d) and averaged over March 1st to 8th (e) and (f) compared to climatology and re-analysis observations; shaded areas in panels a and b indicate the corresponding time periods displayed in c–f.

3.2. Zonal Mean Signatures of Tropospheric and Stratospheric Circulation Extremes

Figures 1a and 1b show the evolution of U_{10}^{60} and $\tilde{AO}$ during early 2020 according to re-analysis data and the ensemble mean of numerical simulations with varying initialization date (mid January to early February). Both the stratospheric and tropospheric circulation are dominated by periods of extreme and persistent positive anomalies compared to the climatology.

A prominent feature in the observed evolution of the stratospheric index (U_{10}^{60}, see Figure 1a) is a period with persistently large values spanning roughly from February 10th to March 20th. The U_{10}^{60} index reaches values up to about 60 m/s during that period and deviations from the climatology temporarily exceed the equivalent of two standard deviations. Prior to this period of elevated values, the observed U_{10}^{60} index shows signs of SSD, with a drop of about 25 m/s within 1 week from about 45 m/s on January 30th to roughly 20 m/s on February 6th (still staying above climatology). However, the stratospheric polar vortex does not stay in this relatively weak state, but rapidly recovers and shows record-high values over the course of the following weeks (e.g., $U_{10}^{60} \approx 60$ m/s on February 17th). The period of persistently extreme positive anomaly ends around March 20th, again showing signs of SSD with the U_{10}^{60} index dropping more than 30 m/s within about 7 days. Due to the rapid recovery of the vortex following the deceleration in early February the U_{10}^{60} evolution does not satisfy the definition of an SSD in Birner and Albers (2017) (drop of 20 m/s within 10 days). However, as we will show in Sections 4 and 5, the February evolution was characterized by an increased likelihood for weak vortex periods associated with substantial vortex decelerations during this period. We will therefore refer to the early February deceleration event as SSD for simplicity.

Various numerical model simulations initialized in January and early February are able to capture some aspects of the described evolution of the polar vortex strength. However, we find a high sensitivity of the ensemble mean to the initialization date. In particular, the observed sequence of events in the stratosphere, including SSD and subsequent strengthening of the polar vortex (due to a WRE; see Section 4) in early February, is not fully reproduced by ensembles with lead times exceeding about 2 weeks (Figure 1). Based on these qualitative differences in prediction skills we can separate the ensembles into three groups with distinct differences in U_{10}^{60} evolution depending on their initialization date: pre-SSD, SSD-onset, and post-SSD.

Ensembles within the pre-SSD group are initialized well before the SSD (January 19th and 22nd) and therefore do not capture the SSD in early February and the subsequent strengthening of the polar vortex. The ensembles in the SSD-onset group, on the other hand, are initialized just before the onset of the SSD (January 25th and 28th). Hence, these experiments capture the SSD deterministically but the corresponding ensemble means do not show clear signs of a pronounced recovery phase. In contrast, ensembles in the post-SSD group are initialized toward the end or after the SSD (January 30th or February 1st and fourth) and deterministically capture many of the aspects of the observed evolution of the U_{10}^{60} index, including a pronounced recovery phase in early and mid February. It seems like ensembles capturing part of the vortex recovery in their respective ensemble mean evolution (i.e., post-SSD ensembles) show a strong persistence in their anomalous polar vortex strength. The distinct differences in behavior of ensembles in the three groups and the corresponding differences in the downward influence on the troposphere are further discussed in Section 5.

In terms of the evolution of the observed tropospheric large scale circulation (Figure 1b) we find two pronounced periods with extremely large positive $\tilde{AO}$ index, peaking at February 9th and 21st with deviations from the climatology corresponding to around three and four standard deviations, respectively. The extreme period around Feb. 9th is to some extent represented deterministically within the post-SSD ensemble simulations, while earlier initializations (pre-SSD and SSD-onset) do not seem to capture this event in their ensemble means. Recall that the ensemble means of experiments in the post-SSD group also deterministically predict the observed evolution of the U_{10}^{60} index (in terms of a strong recovery phase following a SSD; see Figure 1a), suggesting a correlation between these tropospheric and stratospheric events.

The $\tilde{AO}$ index shows persistent positive anomalies during almost the entire winter period, exceeding one climatological standard deviation multiple times. It should be emphasized that the $\tilde{AO}$ index (or equivalently the AO index) has a typical decorrelation time scale of about one or 2 weeks (e.g., E. P. Gerber et al., 2008) and thus the prolonged persistent period of almost entirely positive climatological anomaly in February and March can be regarded as an extreme period in a persistence sense. The predicted $\tilde{AO}$ index seems to be generally larger during late February and March in post-SSD ensembles compared to pre-SSD and SSD-onset ensembles, which suggests a stratospheric influence as post-SSD ensembles also show substantially and persistently increased values of U_{10}^{60} during this period (Figures 1a and 1b might show positive model biases in U_{10}^{60} and $\tilde{AO}$ during March compared to re-analysis data. A quantitative comparison between the model and re-analysis data should therefore be done with caution). The observed $\tilde{AO}$ index drops slightly below climatology at the end of March (not shown) and stays anomalously low for the following weeks, consistent with a drop in AO index toward climatology (see Lawrence et al., 2020). This drop is potentially correlated to the substantial weakening of the polar vortex in mid March.

Figures 1c, 1d and 1e, 1f further emphasize a potential coupling between the stratosphere and troposphere beyond a correlation of ensemble mean behavior. Panel 1c shows how the member distribution of $\tilde{AO}$ on February 9th changes from a generally broad distribution spanning the climatological mean to a narrow distribution spanning the observed value as the initialization date approaches February 9th (and thus the SSD with subsequent vortex strengthening is captured entirely deterministically). However, the predicted U_{10}^{60} index changes rather rapidly with lead time (compared to the typical stratospheric time scale of several weeks). In particular the ensemble initialized on January 25th shows a large fraction of members that predict a weak vortex. This is consistent with the introduced prediction of systematic SSDs (and for some members associated WREs) within the ensembles around the corresponding lead times.

Figures 1e and 1f show the evolution of $\tilde{AO}$ and U_{10}^{60} indices during the later stages of the ensemble simulations (averaged over March 1st to 8th), when the forecast is well beyond the deterministic period and the system has only limited initial conditions memory remaining. Note that pre-SSD and SSD-onset ensembles (i.e., initialized before about Jan. 30th) correspond to rather broad distributions of the stratospheric index that show a significant
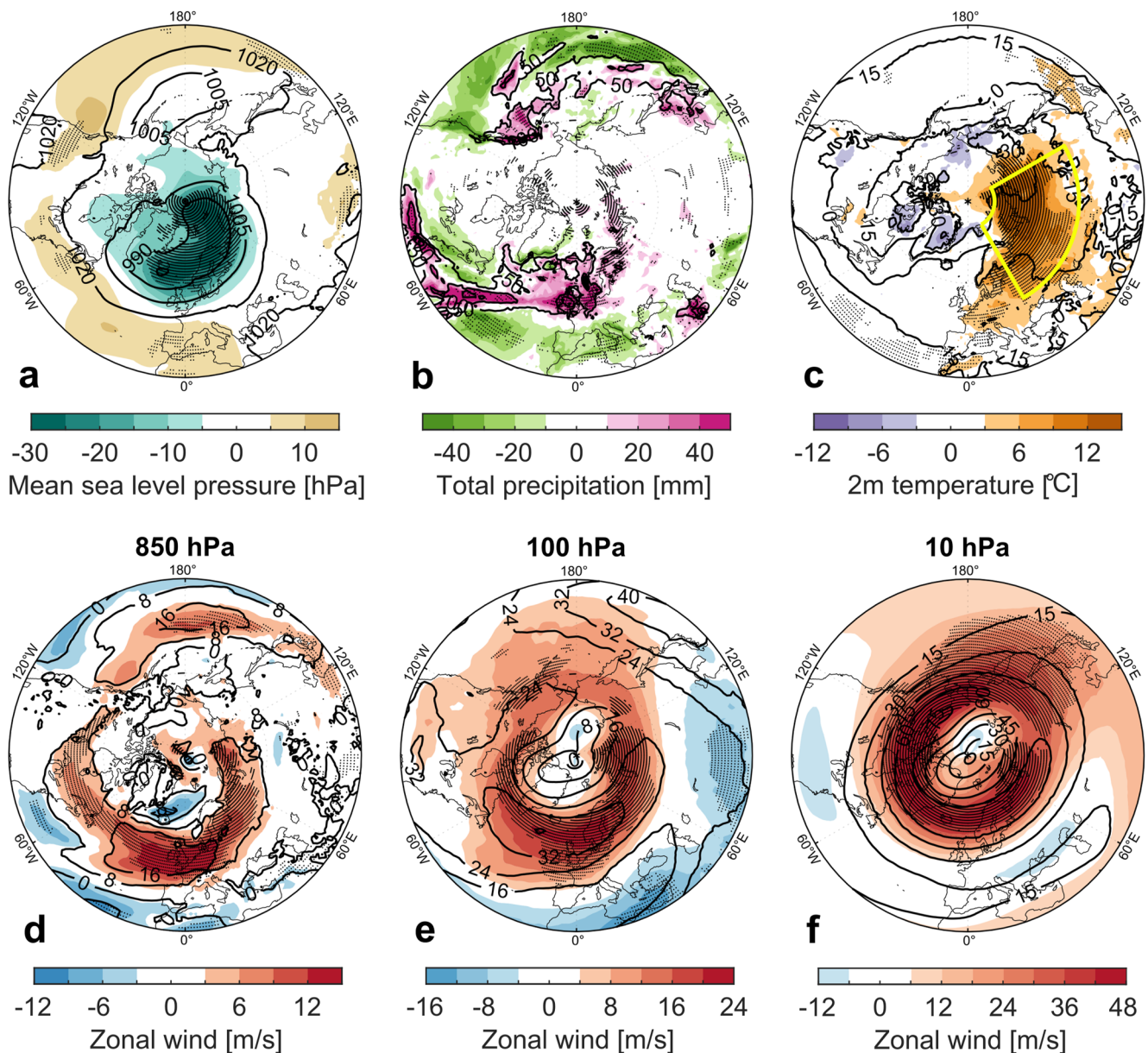
Figure 2. The full re-analysis fields (contours) and climatological anomalies (shading) of mean sea level pressure (a), total precipitation (b), 2m temperature (c) and zonal wind at 850 hPa (d), 100 hPa (e) and 10 hPa (f) averaged over February 15th to 25th. The stippling indicates anomalies above the 95th and below the fifth climatological percentile. The outline in panel c visualizes the region used for clustering in Figure S4 in Supporting Information S1.

amount of members with weak polar vortices (e.g., $U_{10}^{60} < 0$ m/s), while later initializations correspond to much narrower distributions centered around a rather strong polar vortex (large U_{10}^{60}). The member distributions of the tropospheric index also show pre-SSD and SSD-onset ensembles to include a substantial fraction of members with weak tropospheric flow (e.g., $\tilde{AO} < 0$ m), while post-SSD ensembles correspond to relatively strong tropospheric flows only. This is further discussed in Section 6.

3.3. Regional Signatures of Tropospheric and Stratospheric Circulation Extremes

As previously discussed by Lawrence et al. (2020) and Lee et al. (2020), the weather conditions at the surface showed very anomalous characteristics from early February onwards, especially over the North Atlantic and Eurasia. Figure 2 provides an overview of the observed surface conditions and the structure of the polar vortex and

the mid-latitude jet in mid/late February. This period is characterized by an extremely large positive $\tilde{AO}$ index peaking on February 21st (cf. Figure 1). Hence we find strong mean sea level pressure anomalies over the polar cap, and to a lesser extent over the Azores and the North Pacific (Figure 2a). The associated strong meridional pressure gradients are consistent with enhanced westerlies (cf. Figure 2d). The strong westerlies were further associated with a large number of intense storms traveling over the North Atlantic toward Western Europe, whose impact on precipitation is clearly visible in a south-west/north-east rainband across the North Atlantic toward Western Europe (Figure 2b), leading locally to wet and windy conditions during this period. Figure 2c displays a large warm anomaly of 2m temperature, which covers almost entire Eurasia at higher latitudes. This positive anomaly, which is intense and persistent, develops in mid-February and lasts until March (see Figure S1 in Supporting Information S1).

Next, we analyze in more detail the structure of the polar vortex and the mid-latitude jet during February. Figures 2d–2f show the zonal wind anomalies in the troposphere and the lower and upper stratosphere, respectively. After the SSD event in early February, the polar vortex recovered quickly to an extremely strong state. Indeed, the polar vortex is highly symmetric and zonal wind speeds exceed the 95th percentile of the climatological distribution over most of the polar cap (Figure 2f). In the lower stratosphere (100 hPa), the jet over the North Atlantic and Eurasia is significantly enhanced compared to the beginning of February. There are negative zonal wind anomalies over the Mediterranean and Mongolia, reducing the gradients between high and low latitudes. Many of the characteristics of the 10 hPa and 850 hPa winds are also captured at 100 hPa, indicating a strat-trop coupling. In the lower troposphere, the eddy-driven jet extends north-westward to western Europe and the North Sea, resulting in wet and stormy weather in these regions (cf. Figure 2b). Over the Pacific sector, the jet stream is slightly shifted northward compared to climatology but is less anomalous than the Atlantic jet stream. The evolution of both tropospheric and stratospheric fields from January to March (not shown) provides evidence that the anomalous signals develop during or after the recovery from SSD.

As discussed above, the observed tropospheric conditions with strengthened vortex (late Feb. and early Mar.) were characterized by a persistent warm anomaly in surface temperature over the Eurasian continent (Figure 2c). We find a corresponding tropospheric regional temperature signal in certain members of the numerical ensembles simulations (Figure S4 in Supporting Information S1). Members in SSD-onset ensembles (initialized in late January) that show an increased 2-m temperature over Eurasia in late February are generally associated with increased values of $\tilde{AO}$ and correspondingly a stronger mid-latitude jet than members with lower temperature. In addition, warm cluster members show increased values in U_{10}^{60}. The correlation of the surface temperature signal and the polar vortex strength further indicates the importance of strat-trop interactions in early 2020.

4. Wave Reflection Event in Early February and Its Impact on the Stratospheric Circulation

In Section 3.2 we find indications that the evolution of the stratospheric polar vortex during early February 2020 was dominated by a SSD, followed by a pronounced recovery of the polar vortex with persistent and extreme positive stratospheric circulation anomalies that lasted for several weeks. In this section we show that this recovery of the polar vortex was associated with a wave reflection event (WRE). Recall that both types of events, SSDs and WREs, are characterized by anomalous planetary wave-interactions between the troposphere and stratosphere and are therefore associated with anomalous vertical wave activity flux F_p in the lower stratosphere (definition of F_p follows Andrews et al., 1983).

The evolution of F_p during early 2020 is shown in Figure 3 for zonal planetary wave numbers 1 and 2. Wave reflection events can be identified as periods of persistent downward wave activity fluxes preceded by corresponding upward fluxes. We find a clear indication for a WRE in both wave numbers in early February, with initially pronounced upward wave fluxes turning downward around February 10th for wave number 1 and around February 5th for wave number 2. In both instances, the subsequent downward propagating waves reach tropospheric pressure levels (below ca. 200 hPa). Figure 3 further shows the period of enhanced polar vortex strength following the WRE (late February and early March) to be generally characterized by relatively weak tropospheric wave forcing and consequently overall weak upward wave fluxes in the stratosphere, in particular for wave number 1.

The dynamics associated with the WRE in early February, to some extent, can be understood in terms of linear wave theory and wave-mean flow interaction near reflective surfaces. Reflective surfaces are typically associated
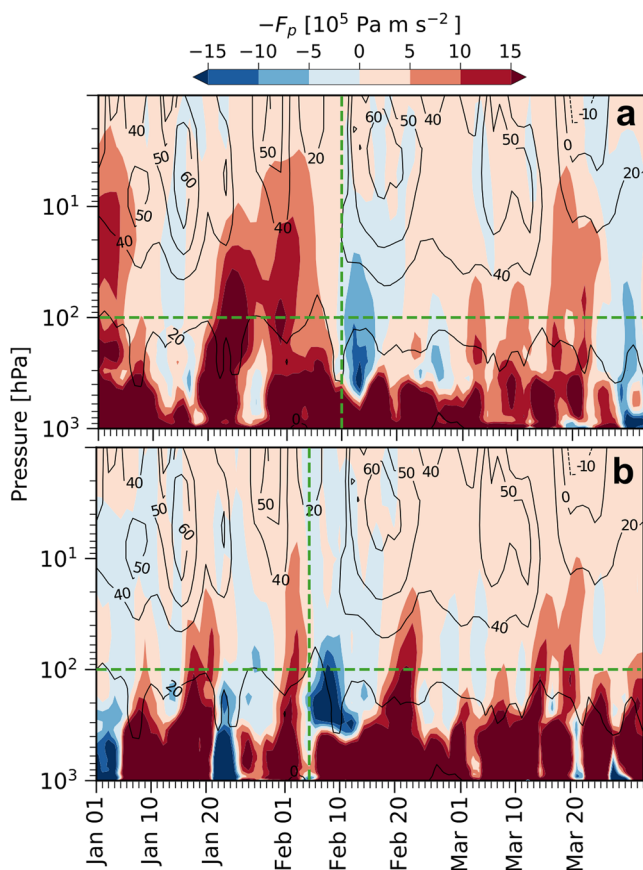
Figure 3. Decomposition into wave numbers 1 (a) and 2 (b) of the vertical component of the upward wave activity flux ($-F_p$) from re-analysis averaged over 45°–75° North. Positive values ($-F_p > 0$, shown in red) correspond to upward wave propagation, while negative values ($-F_p < 0$, shown in blue) correspond to downward wave propagation. Contours depict the zonal mean zonal wind at 60° North. Horizontal dashed lines indicate the 100 hPa level, vertical dashed lines mark the time of sign reversal in F_p at 100 hPa (February 10th and 5h, respectively).

with regions of negative refractive index (see, e.g., Albers & Birner, 2014 for details on how to compute the refractive index), which generally prohibit Rossby wave propagation and hence allow for the reflection of these waves. As shown in Figure 4, the refractive index exhibited an anomalous structure in both early and mid/late February compared to periods with a vortex more similar to climatology (e.g., as in February 2012, shown in Figure 4a for comparison), including pronounced regions of negative refractive index in the mid-latitude and polar stratosphere. In particular, we find two regions in early February at around 40–50°N/100-5 hPa and around 60–80°N/above 20 hPa, acting as meridional and upper boundaries of a vertically confined wave guide at about 60°N. This wave guide further intensifies in mid/late February, making the stratospheric state even more favorable for WREs and potentially helping to maintain the strengthened polar vortex. The configuration of the refractive index in terms of a confined wave guide is consistent with the polar vortex winds during a "split-state", as discussed by Lawrence et al. (2020). We also analyzed the refractive index during early February (time of the onset of WREs) for ensemble clusters that experience no, weak or strong WREs (Figure S2 in Supporting Information S1). We find that the cluster with strong WREs develops generally more pronounced regions of negative refractive index in the mid-latitude middle stratosphere (around 45°N and 10 hPa) and the polar upper stratosphere, acting as a meridional and vertical barriers of the confined wave guide, compared to the cluster without WREs. The details of the vertical and meridional vortex structure play a key role in promoting either reflection or dissipation of upward wave fluxes (also see Figures 4 and 5 and Section. 7). As such, the corresponding vortex structure exhibited in the strong WRE cluster is consistent with the findings of Perlwitz and Harnik (2003) and Shaw et al. (2010).

In order to investigate the effect of the mid February wave reflection on the stratospheric zonal circulation, the members of SSD-onset ensembles (initialized January 25th and 28th) are clustered based on whether they experience a strong and persistent WRE in early/mid February or do not show any signs of a WRE. Here we define strong WREs as periods with downward wave propagation ($-F_p < 0$ at 100 hPa) in both wave number 1 and 2 for at least 4 consecutive days between February 5th and 17th (the periods do not have to occur simultaneously for both wave numbers within the selection period, consistent with the observed WRE in Figure 3). In contrast, we classify a member as not experiencing a WRE in early/mid February if all coherent periods of downward wave propagation (in wave number 1 or 2) last for less than 3 consecutive days. We further define a cluster of (remaining) members with weak WREs, where the lengths of periods with downward flux exceed 2 consecutive days in at least one wave number, but do not exceed 4 consecutive in both. The wave fluxes observed in re-analysis data (Figure 3) satisfy the condition for a strong WRE in early February.

The zonal mean zonal wind at 60° North is depicted in Figure 5 for clusters with strong WRE and no WRE. While both clusters show indications for a SSD experienced at the beginning of February, the ensemble members with strong wave reflection display a substantial recovery in the stratosphere thereafter, with a similarly strong and persistent stratospheric polar vortex as seen in the re-analysis data (e.g., wind speeds exceeding 40 m/s at 10 hPa in late February; see Figure 1). A much weaker stratospheric polar vortex is seen for the ensemble members with no WRE, suggesting a strong coupling of lower stratospheric wave fluxes to the polar vortex strength.

The substantial differences in polar vortex strength between the clusters are also visible in Figure 6a, which depicts the stratospheric response relative to the onset of the wave reflection (time of first sign reversal in F_p in either wave number). It can further be seen that none of the members in the strong WRE cluster shows signs of a SSW (in terms of $U_{10}^{60} < 0$) and the inter-member variability in this cluster is relatively small. In contrast, members in the cluster without WRE span a large range of vortex strengths following the event, including several
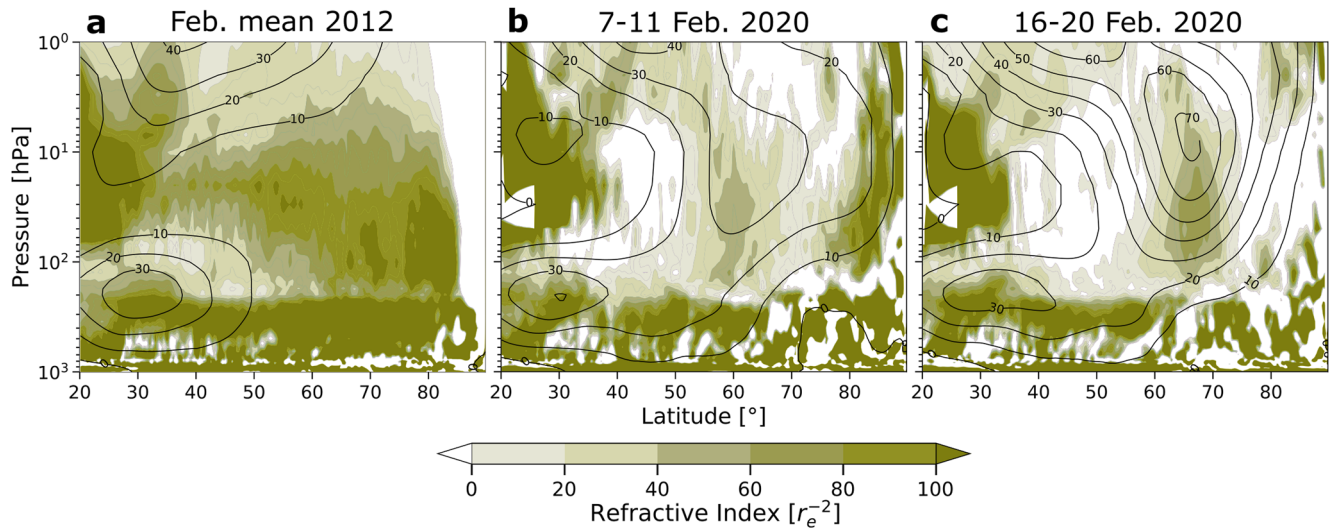
Figure 4. Zonal mean quasi-geostrophic refractive index n^2 (shading) and zonal mean zonal wind at 60° North (contours) in re-analysis data, averaged over different time periods. The refractive index has been calculated for stationary waves with zonal wave number 1 and zero intrinsic phase speed and is non-dimensionalized with the Earth's radius of r_e.

members with pronounced SSW. Note here that the weak WRE cluster mean also shows a relatively weak recovery in polar vortex strength following the SSD in early February, and consequently, moderate stratospheric zonal wind speeds in the following weeks compared to the clusters with strong WRE and no WRE.

While significant differences in the cluster means are visible in the stratosphere, the tropospheric signal is less robust. We find a systematic difference in the $\tilde{AO}$ values between the cluster with strong WRE and the cluster without WRE for about 2 weeks following the event. This difference in $\tilde{AO}$ appears to be mostly associated with the weakening of the tropospheric circulation following the weakening of the vortex due to SSWs, rather than the strengthening of it due to WREs. Correspondingly, we do not find any difference in $\tilde{AO}$ between the clusters with strong and weak WREs. Overall, these results indicate that the mid February WRE in the stratosphere on its own did not exhibit a direct downward influence on the tropospheric zonal mean circulation. We address this once more in Section 7.
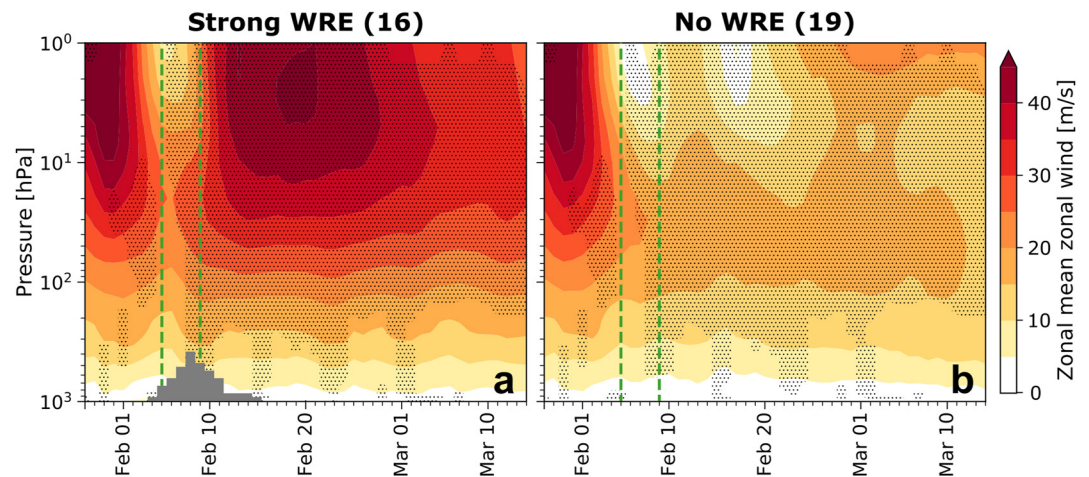

Figure 5. Evolution of zonal mean zonal wind at 60° North for clusters with strong wave reflection during the period February 5th to 17th and without persistent wave reflection in a lagged stratospheric deceleration-onset ensemble (initialized January 25th and 28th). The stippling indicates significant differences (to 95% confidence) in cluster means and numbers in the panel headings represent cluster sizes. Vertical dashed lines mark the times of observed WREs in wave numbers 1 and 2. The histogram at the bottom of panel a indicates the number of wave reflection events occurrences (wave numbers 1 and 2 counted individually) in the strong WRE cluster, with a peak of 13 events in February 8th.
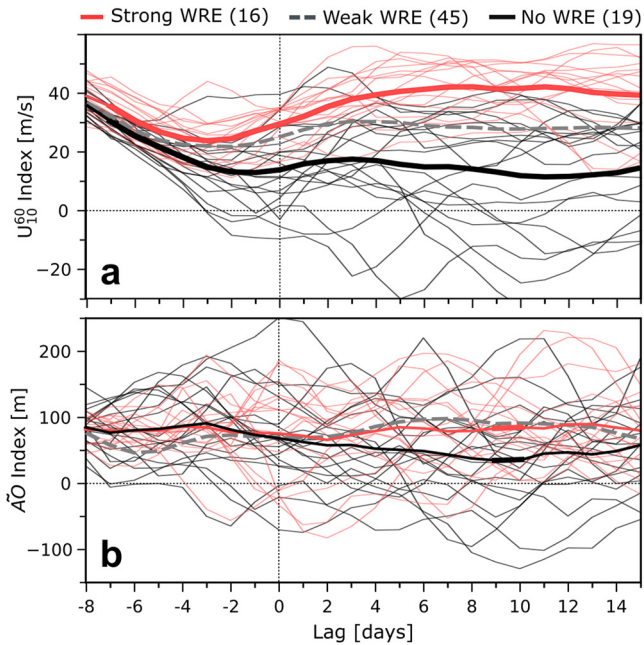
Figure 6. Lagged composite evolution of U_{10}^{60} and $\tilde{AO}$ indices for clusters with strong wave reflection and without reflection, respectively, for a lagged stratospheric deceleration-onset ensemble (initialized January 25th and 28th). The event day is defined as the first day of sign-change in either the wave number 1 or 2 component of F_p at 100 hPa for the wave reflection cluster, and as February 10th for the no wave reflection cluster (the day of sign-change in the wave number 1 component of F_p at 100 hPa in re-analysis data). The cluster mean is shown for all clusters, individual members are also shown for the strong and no wave reflection event (WRE) clusters. Thick line segments indicate a statistically significant difference in means between clusters with strong and no WRE (to 95% confidence). Numbers in the legend indicate cluster sizes.

5. Downward Coupling Following the Wave Reflection Event in Early February

5.1. Sensitivity of Predictability and Coupling on Initialization Period

As shown in Section 3 February 2020 was characterized by two periods of extreme $\tilde{AO}$ index (peaking February 9th and 21st) as well as an abrupt increase of the polar vortex strength following a SSD in early February, leading to extremely elevated values of U_{10}^{60} that persisted for over a month. We further show in Section 4 that this strengthening of the polar vortex in early February was associated with a WRE. March 2020, on the other hand, was mostly characterized by persistently positive values of both $\tilde{AO}$ and U_{10}^{60}. This section aims to analyze the coupling between the anomalous tropospheric ($\tilde{AO}$) and stratospheric (U_{10}^{60}) development in the period following the WRE. As part of this analysis we study whether the tropospheric extremes observed in February were more likely to occur due to the WRE directly, or secondly due to the anomalously strong and persistent polar vortex.

First, we examine whether the tropospheric $\tilde{AO}$ anomalies in mid/late February are linked to the polar vortex strength in general. To do so, we consider a very large ensemble of 320 members utilizing 8 initialization dates between late January and early February, hence including ensembles from all three groups (pre-SSD, SSD-onset and post-SSD) defined in Section 3. In Figure 7 ensemble members have been separated into two clusters based on whether they do or do not show extreme values in $\tilde{AO}$ in mid/late February, where extremes are defined as $\tilde{AO}$ exceeding 140m for at least one day between February 15th and 25th (the threshold of 140m roughly corresponds to the 85th-percentile of the member distribution at any given time step; the time period in mid/late February corresponds to a period with extremely increased observed $\tilde{AO}$ and lies sufficiently far outside of the deterministic period). The two clusters not only show significantly different $\tilde{AO}$ values during mid/late February (by definition), but also several days before and after this period (see Figures 7a and 7c). In particular we find significantly increased $\tilde{AO}$ around February 9th, that is, during the time of the first observed $\tilde{AO}$ extreme and the stratospheric wave reflection event (keep in mind that for some of the ensembles included in Figure 7 early February lies within the deterministic period, hence cluster means should be interpreted with care near the beginning of the shown period).

Figures 7b and 7d also show significant differences between the two clusters in terms of the U_{10}^{60} index. Since the clusters have been formed purely based on the tropospheric evolution (with and without $\tilde{AO}$ extreme in mid/late Feb.), any stratospheric differences suggest a strat-trop coupling. The stratospheric signal within the lagged ensemble shown in Figure 7 consists of a relatively weak (about 8 m/s) but very persistent positive anomaly in terms of U_{10}^{60} cluster difference. Only a very small fraction of members within the cluster with mid-February $\tilde{AO}$ extreme experiences a SSW over the course of the integration ($\approx 8\%$ compared to $\approx 21\%$ of members without $\tilde{AO}$ extreme).

After having established the link of stratospheric anomalies and tropospheric extremes in a general sense by averaging over all available ensembles in Figure 7, we now turn to the question of how the coupling of the strat-trop flow evolved over the period of interest. Therefore, we analyze cluster differences in $\tilde{AO}$ and U_{10}^{60} for each individual ensemble with varying initialization date (Figure 8). In particular, the evolution of U_{10}^{60} is consistent with the grouping of these individual ensembles into the three groups (pre-SSD, SSD-onset, and post-SSD) defined in Section 3. Although the variability within individual ensembles can be very large, circulation anomalies evolve consistently within the respective groups. For pre-SSD ensembles the cluster with $\tilde{AO}$ extreme shows a relative strengthening of the stratospheric circulation (positive difference in U_{10}^{60} cluster mean) in early February compared to the cluster without $\tilde{AO}$ extreme. This circulation anomaly persists well into mid March. In SSD-onset ensembles the positive mean U_{10}^{60} cluster difference is limited to about a week prior to the $\tilde{AO}$ extreme around
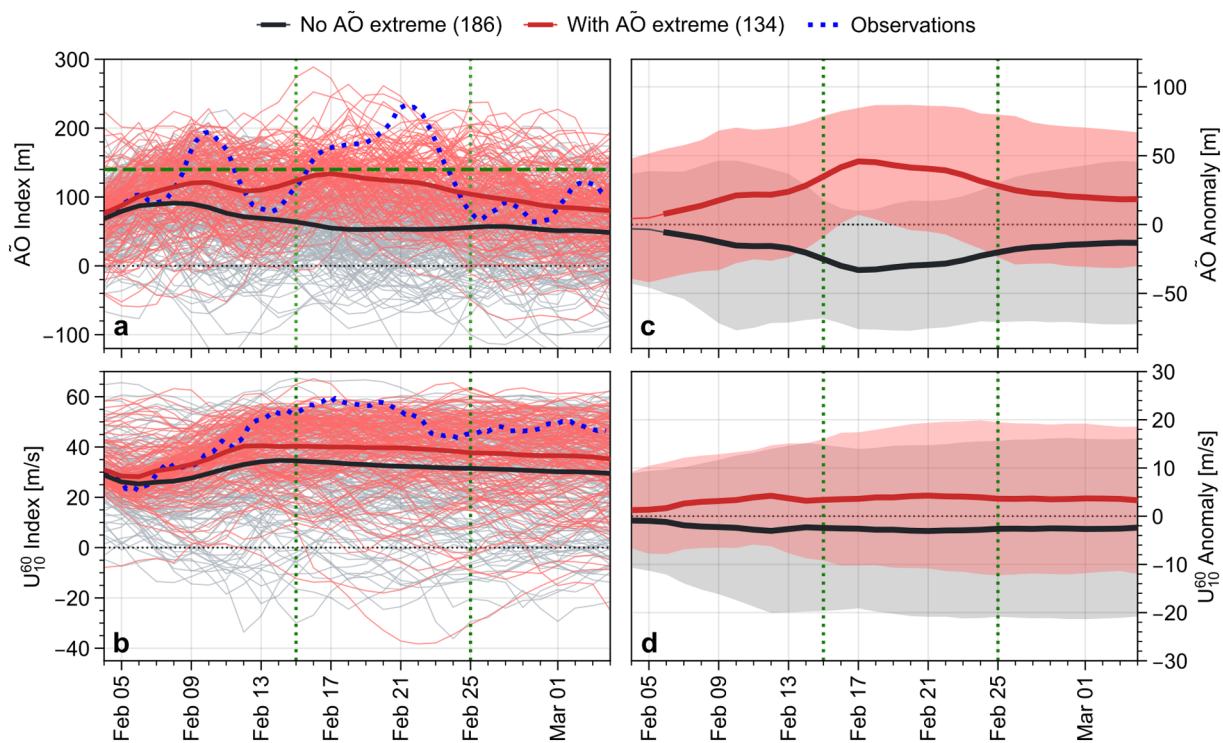
Figure 7. Evolution of U_{10}^{60} (top) and $\tilde{AO}$ (bottom) indices for a lagged ensemble with 8 initialization dates between January 16th and February 4th. Members are clustered based on whether $\tilde{AO}$ does or does not exceed 140m for at least one day between February 15th and 25th with cluster sizes indicated with bracketed numbers. Subplots a and b show full indices, thin lines represent individual members and thick lines represent the respective cluster means. Subplots c and d show the deviation from the ensemble mean, where lines represent the cluster means, the shading indicates cluster variability in terms of one standard deviation and thick line-segments indicate periods, where the difference in cluster means, is statistically significant (to 95% confidence). The dotted lines show re-analysis data for 2020. Vertical dotted lines indicate the time period for the clustering criterion, the horizontal dashed line in subplot b indicates the threshold of 140m. Bracketed numbers in the legend indicate the number of members in the respective cluster (out of 320 in total).

Feb 21st, that is, the period of strong vortex recovery in the observations. This is consistent with essentially all SSD-onset ensemble members predicting the SSD, but only part of them the recovery. Post-SSD ensembles, on the other hand, do not show any significant difference in U_{10}^{60} between the clusters throughout the simulation. The lack of difference is due to the fact that essentially all ensemble members simulate a strong and persistent polar vortex (see Figure 1). Thus, SSD-onset ensemble members are most suitable to study the coupling between stratospheric and tropospheric flow for the specific evolution in February 2020, and they will be further analyzed in Section 5.2.

The distinctly different stratospheric evolution of ensembles seen in Figures 1 and 8 is consistent with a change in predictive skill for the clustering period with advancing initialization date. As discussed in Section 4, the stratospheric dynamics in early 2020 was characterized by SSD around Feb. 6th induced by upwards propagating planetary waves, followed by a stratospheric WRE leading to an anomalously strong polar vortex for several weeks. Depending on the initialization date, a fraction of ensemble members in a given ensemble is able to predict either the entire sequence of stratospheric events (SSD followed by WRE and persistently strengthened vortex) or only certain aspects of this sequence. This behavior is summarized in Figure 9, showing an increased probability for a weak polar vortex to occur in early February for initialization dates in the SSD-onset period (around January 25th). In contrast, ensembles initialized in the post-SSD period predict a generally strong polar vortex in early/mid February, consistent with an increased fraction of members that predict a WRE.

Figure 9 also shows the chance for extreme events with increased $\tilde{AO}$ to occur on February 9th and 21st, that is, the periods with observed extreme values. The likelihood for extreme $\tilde{AO}$ events on February 9th seems to increase during the post-SSD period (consistent with the initialization date approaching the time of the observed $\tilde{AO}$ extreme), although only after the chance for a WRE in early February increases. The chance for an $\tilde{AO}$ extreme on Feb. 21st is generally small (consistent with the long lead times) with ensembles initialized in the
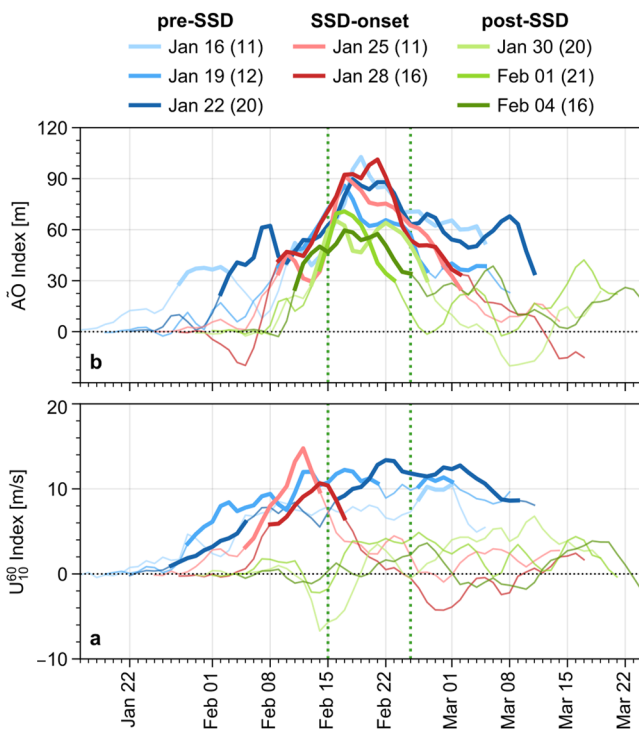
Figure 8. Difference in U_{10}^{60} (top) and $\tilde{AO}$ (bottom) indices between clusters from ensembles with varying initialization date between January 16th and February 4th. Clusters were formed based on whether $\tilde{AO}$ does or does not exceed 140m for at least one day between February 15th and 25th. Thick line segments indicate periods for which the difference in cluster means is statistically significant (to 95% confidence). Vertical dotted lines indicate the time period for the selection criterion. Bracketed numbers in the legend indicate the number of ensemble members (out of 40 per ensemble) that exceed the threshold.

SSD-onset period appearing to show a low likelihood in particular, potentially indicating a downward influence of the generally weakened polar vortex characterizing these simulations. Further, the chance for an $\tilde{AO}$ extreme on Feb. 21st seems generally higher for post-SSD ensembles compared to pre-SSD ensembles, further suggesting a downward coupling of the strengthened polar vortices in post-SSD members (cf. Figure 1). However, the likelihood for an extreme event on Feb. 21st in Figure 9 should be interpreted with caution since it is not fully clear to what extent any differences go beyond natural climatological variability or to what extent the increased likelihood for ('transition') initializations Jan. 22nd and 28th is significant.

5.2. Evolution in Pre-SSD Ensembles

Figures 1 and 7 suggest a downward influence of a strengthened stratospheric polar vortex (following a WRE) on the troposphere and hence a contribution to the formation of observed extreme $\tilde{AO}$ values in late February. The extent to which this potential downward influence is captured in ensemble members depends on the initialization time (pre-SSD, SSD-onset or post-SSD periods; see Figures 8 and 9). The pre-SSD ensembles do not capture the specific stratospheric evolutions of the SSD and WRE, but still show a statistical relation of the occurrence of tropospheric extremes to the stratospheric polar vortex strength. For example, Figure 8 shows a clear difference in U_{10}^{60} cluster mean when clustering pre-SSD ensemble members based on whether they exhibit an $\tilde{AO}$ extreme in late February.

However, if we perform the same clustering, but exclude all members that experience a weak polar vortex at any point in time (Figure 10), the stratospheric difference between both clusters essentially disappears and both clusters show equally large values of U_{10}^{60} throughout February, while the tropospheric anomaly in late February remains almost unchanged. This behavior of the clusters suggests that the strat-trop coupling signal seen in Figures 7 and 8 (i.e., the correlation of stratospheric and tropospheric circulation anomalies) is almost entirely caused by members predicting a weak polar vortex rather than by members that predict an anomalously strong vortex.

We find a similar tropospheric signal when clustering pre-SSD ensemble members based on the strength of their stratospheric zonal circulation in early February (Figure S3 in Supporting Information S1). Members with a stronger polar vortex in February correspond to a generally increased $\tilde{AO}$ index. However, clusters associated with a generally strong or moderate polar vortex strength do not show a clear difference in terms of $\tilde{AO}$ in mid/late February. This is consistent with Figure 10 in the sense that it is rather the lack of the occurrence of a weak vortex than an anomalously strong vortex that explains the tropospheric signal. As such, this indicates an asymmetry in the downward influence of strong versus weak polar vortex situations, which will be further discussed in Section 7.

5.3. Evolution in SSD-Onset Ensembles

The evolution of the stratospheric polar vortex and the downward coupling changes in some respect when considering a lagged ensemble initialized during the SSD-onset period (January 25th and 28th). These ensembles mostly capture the SSD in early February but not fully capture the WRE (as discussed earlier in this section and in Sections 3 and 4). The corresponding ensemble members therefore differ substantially in terms of if and how strong the polar vortex recovers following the SSD. Figure 11 shows three clusters of ensemble members clustered based on their mean U_{10}^{60} index between February 8th and fifteenth. All three clusters experience a pronounced drop in stratospheric circulation in early Feb, but the U_{10}^{60} index of the cluster with strong vortex quickly recovers and reaches values exceeding 45 m/s in mid February, while the U_{10}^{60} index of the cluster with a weak
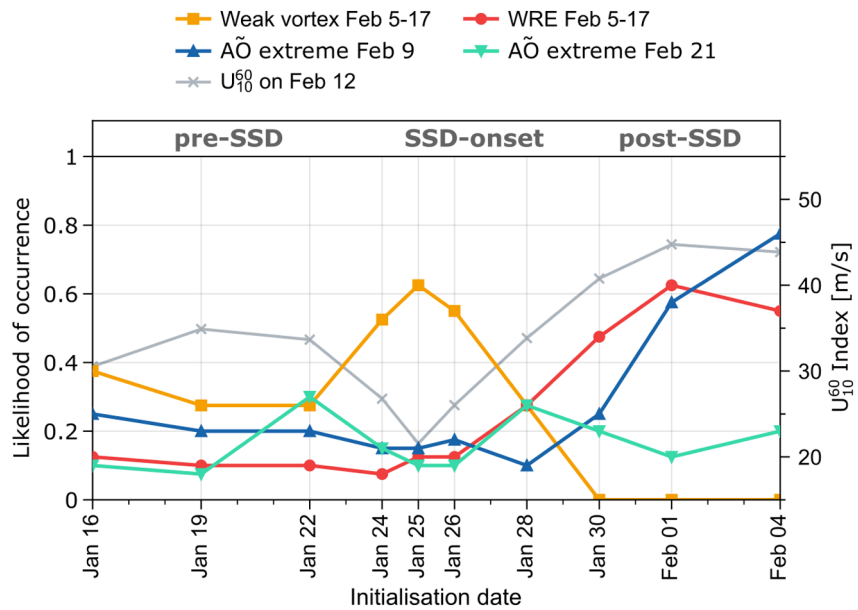
Figure 9. Different probabilities for atmospheric behavior (in terms of member fraction) as a function of initialization date. Shown are the likelihood for extreme events with $\tilde{AO} > 140m$ on February 9th and 21st, for a weak polar vortex with $U_{10}^{60} < 15m/s$ any time during February 5th and 17th and for a WRE ($F_p > 0$ at 100 hPa for at least 5 consecutive days in wave number components 1 and 2, see Section 4) to occur during February 5th and 17th. Also shown is the ensemble mean of U_{10}^{60} (corresponding to the left y-axis, all other metrics correspond to the right y-axis).

vortex keeps dropping and stays persistently below 20 m/s for February and early March. This behavior of the different clusters is consistent with the idea that some members capture the wave reflection event in mid February, while others do not (Correspondingly the U_{10}^{60} evolution of the three clusters is similar to the cluster composite formed based on vertical wave fluxes seen in Figure 6.).

The distinct evolution of the stratospheric zonal circulation in the three clusters allows us to study its potential influence on the tropospheric zonal mean circulation (Figure 11b), which does not show a significant difference between the clusters up to about February 15th (the end of the period used for cluster definition and toward the end of the wave reflection event). However, during the second half of February and early March, the clusters differ significantly in their $\tilde{AO}$ indices, with the strong vortex cluster showing a strengthened tropospheric circulation compared to the weak vortex cluster. Note that the cluster with moderate vortex also shows moderate values of $\tilde{AO}$, even during early March, when the clusters with strong and moderate vortex are almost identical in terms of mean U_{10}^{60} index. It should be noted that the evolution of circulation anomalies at 100 hPa (lower stratosphere) between the three clusters (not shown) is qualitatively similar to the evolution at 10 hPa. The correlation between the stratospheric and tropospheric jets is further emphasized in Figure 11c, which shows the normalized member distributions of various characteristics of the $\tilde{AO}$ indices of the three clusters defined based on U_{10}^{60} evolution. We find a clear difference between the three clusters in all characteristics. In particular, the cluster with a strong vortex shows significantly increased values in persistence and extreme $\tilde{AO}$ metrics compared to the cluster with moderate vortex. Note here that the difference between members with strong and moderate stratospheric flows seems in general much less robust than the difference between weak and moderate flows (cf. Figures 6, 10, and S3 in Supporting Information S1). As further discussed in Section 7 the lack of a robust and clear coupling signal (e.g., when comparing situations with strong and moderate vortex) emphasizes the probabilistic nature of the coupling and indicates an asymmetric downward influence of positive and negative anomalies in polar vortex strength.

The clustering approaches used in this section strongly rely on the underlying ensemble to sufficiently sample a range of possible evolutions of the stratospheric and/or tropospheric circulation. A similar analysis of post-SSD ensembles is therefore much less meaningful, as corresponding members do systematically capture the WRE in early February and therefore produce a generally strengthened polar vortex in the following weeks.
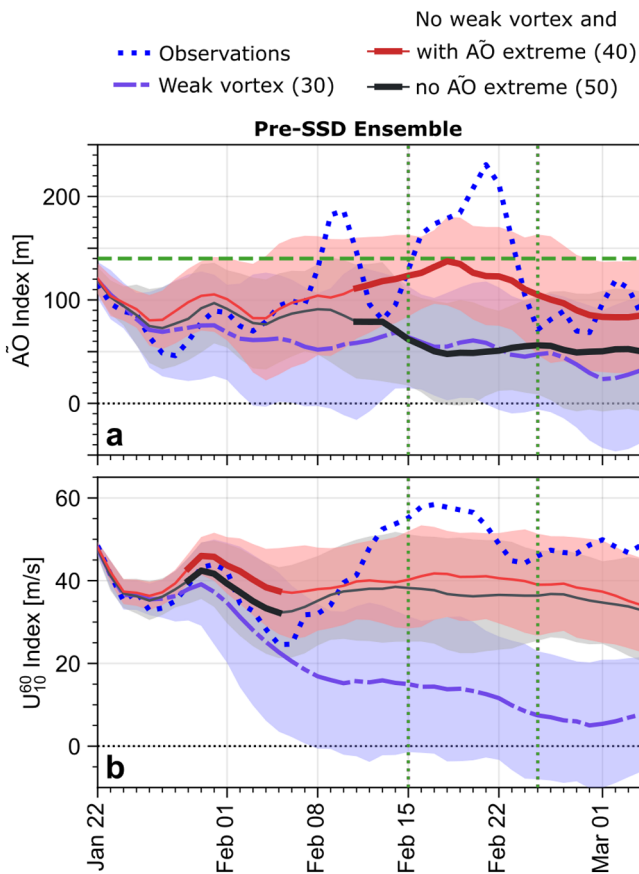
Figure 10. Cluster mean evolution in $\tilde{AO}$ (a) and U_{10}^{60} (b) indices in a lagged pre-SSD ensemble (initialized January 16th, 19th, and 22nd). The three clusters contain members that either experience a weak vortex (defined as $U_{10}^{60} \leq 5$ m/s at any time during the 50 days integration) or do not correspond to a weak vortex but either have an $\tilde{AO}$ extreme (same criterion as used in Figure 7; threshold and periods indicated by horizontal and vertical lines) or do not have such an extreme between February 15th and 25th. The dotted lines show re-analysis observations for 2020, shaded areas indicate cluster variability in terms of one standard deviation, and numbers in the legend show cluster sizes.

6. Influence of the Polar Vortex Strength on Tropospheric Extreme Events

We showed that the specific stratospheric evolution in 2020 with the SSD followed by a WRE and a persistently strong polar vortex potentially contributed to persistent positive $\tilde{AO}$ anomalies in February and March (based on the SSD-onset ensembles, Section 5.3), but also found a more general relation between the stratospheric polar vortex strength and $\tilde{AO}$ extremes (based on pre-SSD ensembles, Section 5.2). This section aims to analyze this general stratospheric influence on $\tilde{AO}$ extremes in situations with a persistently strong or weak polar vortex, irrespective of the specific evolution in February 2020. In particular, we analyze whether persistent stratospheric anomalies impact the persistence, strength and likelihood of tropospheric extreme events (here persistence is associated with the life time of a coherent anomaly exceeding typical time scales of the respective atmospheric layer). We first perform the analysis for a lagged ensemble initialized in mid February, hence covering the time period of interest in March with persistently increased observed $\tilde{AO}$ and U_{10}^{60} indices, but later show that our results are insensitive to the initialization date.

To obtain a general idea of how the tropospheric zonal circulation is influenced by persistent stratospheric anomalies (and vice versa), we analyze three sets of two distinct clusters in terms of the difference in their respective cluster means. In each set members of a lagged ensemble are separated into two clusters based on whether they do or do not correspond to a persistently strong zonal circulation in either the troposphere, the lower stratosphere or the middle/upper stratosphere, corresponding to the three indices $\tilde{AO}$, U_{100}^{60} (defined as zonal mean zonal wind at 60° North and 100 hPa) and U_{10}^{60}, respectively. The differences in cluster means of the three sets are shown in Figure 12. We find that even though persistent positive anomalies in the middle/upper stratosphere show a significant response in the lower stratosphere, they do not appear to induce any significant signal in the troposphere. In a similar way persistent circulation anomalies in the troposphere are correlated to a strengthened lower stratospheric flow, but not to anomalies in the middle/upper stratosphere. Consistently, anomalies within the lower stratosphere show a significant signal in both the troposphere and the middle/upper stratosphere.

Figure 12 suggests there is no direct influence of persistent middle/upper stratospheric flow anomalies on the tropospheric circulation in terms of ensemble means. However, the stratospheric state can still have an effect on individual tropospheric extreme events, which is not apparent in averages over many events as they, for example, might happen at different times or correspond to a combination of positive or negative tropospheric flow anomalies. To study the influence of stratospheric conditions on certain tropospheric extremes, Figure 13a shows a composite of tropospheric events with substantially increased $\tilde{AO}$ index during March. Consistent with Figure 12, we do not find a significant signal in the middle/upper stratosphere correlated to tropospheric extremes, but the lower stratosphere shows slightly elevated values in U_{100}^{60} for roughly a week following the tropospheric extreme (indicative of upward coupling). Figure 12 indicates that flow anomalies in the lower stratosphere can couple to anomalies in both the troposphere and middle/upper stratosphere. Any positive downward influence of a strengthened middle/upper stratospheric circulation on the troposphere should therefore be associated with strong lower stratospheric circulation anomalies, while the downward influence of weakened middle/upper stratospheric circulation on positive tropospheric flow anomalies should be characterized by weakened (or even negative) lower stratospheric anomalies. Correspondingly, if we divide the group of events in Figure 13a into two clusters based on whether the lower stratosphere corresponds to a generally positive or negative ensemble anomaly following the event (Figures 13b and 13c), we
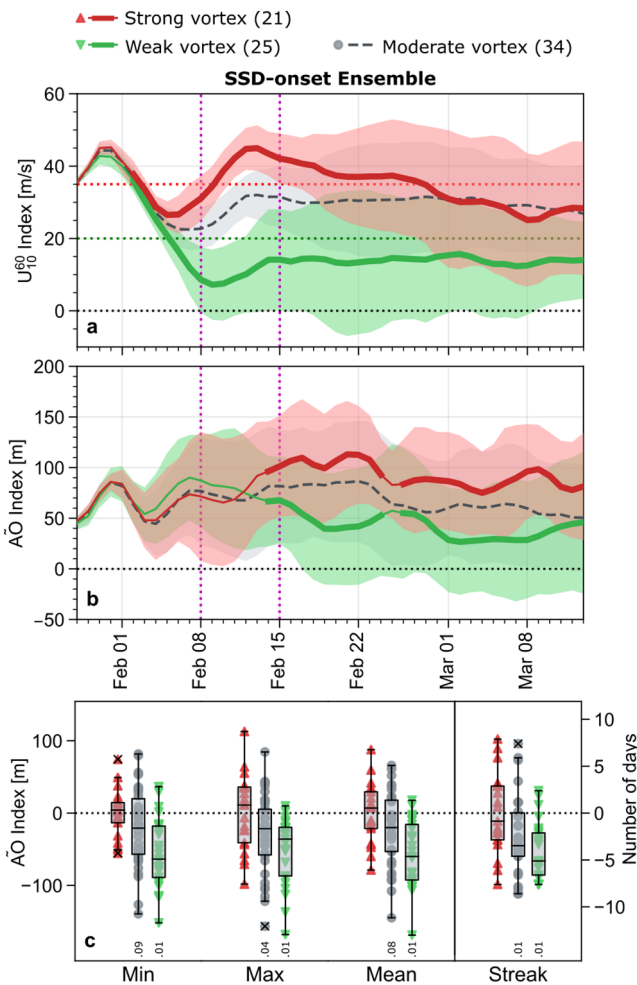
Figure 11. Evolution of U_{10}^{60} (a) and $\tilde{AO}$ (b) indices for a lagged stratospheric deceleration-onset ensemble (initialized on January 25th and 28th). Members are separated into 3 clusters based on whether their U_{10}^{60} index averaged between February 8th and 15th is above 35 m/s (strong vortex), between 20 m/s and 35 m/s (moderate vortex) or below 20 m/s (weak vortex). The curves show the cluster means, with thick line segments for the clusters with strong and weak vortex indicating statistical significant (to 95% confidence) differences between the corresponding cluster means. Shading indicates cluster variability in terms of one standard deviation, vertical dashed lines show the time period used for the clustering, the horizontal dashed lines in subplot indicate the thresholds of 20 m/s and 35 m/s, and numbers in the legend represent cluster sizes. Panel c shows the normalized member distributions of the three clusters for the minimum, maximum, and mean $\tilde{AO}$ between February 15th and 25th, as well as the maximum number of consecutive days with positive $\tilde{AO}$ anomaly between February 15th and Mar. 14th. All member distributions are normalized so zero corresponds to the mean of the cluster with a strong vortex and numbers at the bottom show the p-values for significance tests assuming the mean of clusters with medium and weak vortex to be zero.

find both clusters to show substantial differences in terms of the evolution of their stratospheric and tropospheric circulation.

In particular, we find the positive $\tilde{AO}$ extremes to be significantly stronger and more persistent in the case with positive stratospheric flow anomalies. It should be noted that the two clusters already differ significantly in terms of middle/upper stratospheric circulation more than a week prior to the event date and thus before cluster differences in $\tilde{AO}$ develop. This difference in U_{10}^{60} prior to the start of the event can be interpreted in the way that such tropospheric (extreme) events do occur in situations with both strong or weak polar vortex simply due to internal tropospheric variability, but that the probability distribution and evolution of these events can be significantly modified by the state of the stratosphere at the time of their occurrence. Further, Figure 13 indicates that stratospheric anomalies, in return, respond to the changes in tropospheric circulation, leading to a mutual amplification of the flow anomalies in both layers.

The general modification of tropospheric events by the stratospheric state is a rather robust result within our set of ensembles. Table 1 summarizes the modification of positive and negative $\tilde{AO}$ extreme events by the stratospheric state as an average over multiple ensembles (corresponding values for individual ensembles can be found in the Figure S5 in Supporting Information S1). The event persistence is estimated in terms of the e-folding time of a Gaussian profile fitted to the $\tilde{AO}$ anomaly time series at positive lags of each individual event in the respective group (To be precise the persistence time scale is given by the parameter τ calculated via a least-squares fit of the regression model $\sqrt{-\ln \tilde{AO}_a(\lambda)/\tilde{AO}_a(0)} = \lambda/\tau + \epsilon(\lambda)$, where λ represents time lag, $\epsilon(\lambda)$ is the regression error function, $\tilde{AO}_a(\lambda)$ is the ensemble anomaly of the $\tilde{AO}$ index and the regression is performed for all positive lags $\lambda \geq 0$ for which $\tilde{AO}(\lambda) > 0$; other ways to estimate the event persistence gave qualitatively similar results).

In situations with an anomalously strong lower stratospheric flow (positive U_{100}^{60} anomaly) we find positive $\tilde{AO}$ extreme events to be stronger and longer-lasting. Furthermore, these positive $\tilde{AO}$ anomaly events are more frequent than in situations with a weak polar vortex, which is consistent with an increase in event magnitude due to a shift in probability distribution when considering the definition of events based on a fixed $\tilde{AO}$ threshold. In return, when considering periods with an anomalously low $\tilde{AO}$ index, we find that a strengthened stratospheric polar vortex has a suppressing influence, with the corresponding negative tropospheric events occurring less often, being weaker and lasting considerably shorter (these results are consistent with the findings of, e.g., Charlton-Perez et al., 2018).

Qualitatively, similar characteristics of strat-trop coupling as seen in Figure 13 can be found when analyzing cluster composites-based SSDs (not shown). In particular, our analysis shows no significant deviation from the ensemble mean in $\tilde{AO}$ when averaging over all SSD events occurring in a large lagged ensemble covering February and March 2020. However, we find a significant correlation with the tropospheric jet strength when distinguishing members that are associated with either anomalously strong or weak zonal circulations in the lower stratosphere during/after the SSD. Members associated with an

overall strong stratospheric circulation exhibit a general strengthening of the tropospheric circulation for more than a week following the event. Consistently strong vortex members show a significant increase in magnitude and likelihood of positive $\tilde{AO}$ extremes (and a corresponding decrease in magnitude and likelihood of negative $\tilde{AO}$ extremes) compared to members with anomalously weak lower stratospheric circulation.
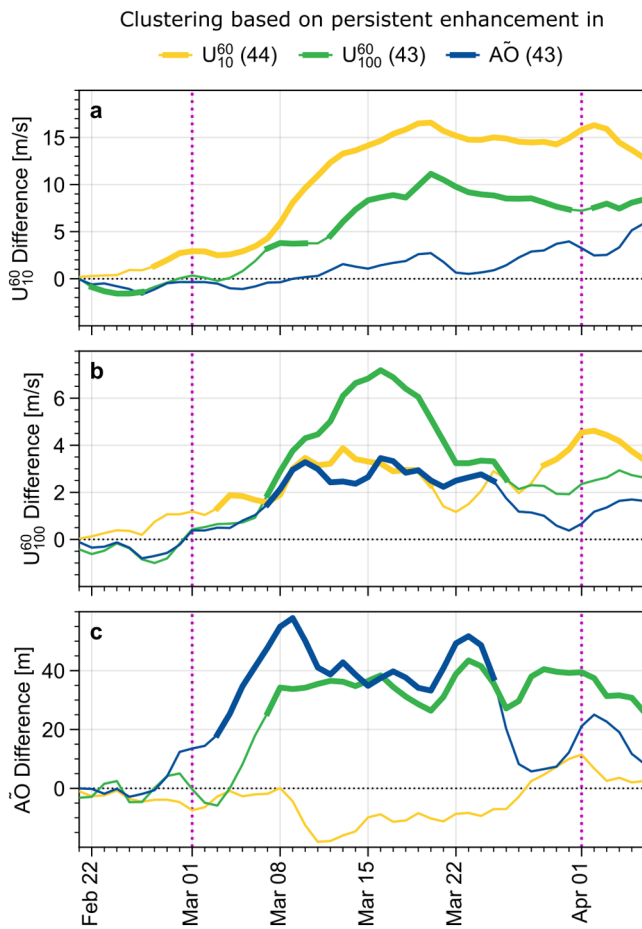
Figure 12. Evolution of the difference in U_{10}^{60}, U_{100}^{60} and $\tilde{AO}$ cluster means in a lagged post-stratospheric deceleration ensemble (initialized February 18th and 21st) for three sets of two clusters (represented by different line colors). The clusters are formed based on one of three criteria, distinguishing members that do or do not show persistently enhanced values in either of the three plotted indices. The three different sets of clusters are based on members that have $U_{10}^{60} \geq 35$ m/s for at least 20 consecutive days, $U_{100}^{60} \geq 20$ m/s for at least 20 consecutive days or $\tilde{AO} \geq 80$m for at least 10 consecutive days within the time period March 1st to April 1st. Thick line segments indicate periods for which the cluster means of each set are significantly different in the respective index (to 95% confidence) and numbers in brackets show how many members (out of 80) satisfy the respective criterion.

7. Discussion

We have shown that the stratospheric evolution in early 2020 was characterized by strong wave-mean flow interaction, including by SSD in early February followed by a WRE that induced strong persistent polar vortex conditions. How well this behavior is captured by ensemble predictions strongly depends on the initialization date, and correspondingly the stratospheric evolution was difficult to predict at certain times (see Figure 1). Such behavior is consistent with the 'bifurcation' of wave propagation properties at critical lines within the stratosphere (e.g., Noguchi et al., 2016; Perlwitz & Graf, 2001), for example, during the SSD (and subsequent WRE) in early February. These bifurcations can lead to a very wide range of potential evolutions of the stratospheric circulation, depending on the interaction of upward propagating waves with the zonal mean flow. While the ensembles initialized around January 25th capture the tropospheric wave forcing in terms of upward wave fluxes in early February and the following SSD deterministically, for some members the stratosphere enters a 'reflecting state', and for other members, it enters (or remains in) an 'absorbing state'. We find the reflective state to be characterized by a well defined wave guide which is vertically and meridionally confined by pronounced regions of negative refractive index, making the stratospheric response to the incoming wave flux (Figure 4 and discussion) sensitive to the details of the vertical and meridional vortex structure. Consistently, SSD-onset ensembles predict a large likelihood for a weak vortex or even SSW in early/mid February (Figure 9).

WREs can occur for both single or multiple planetary wave numbers, and the evolution of the polar vortex strength is generally sensitive to the precise details of the reflection. Correspondingly, members within the SSD-onset ensembles show a very wide spectrum of polar vortex evolutions, ranging from the upward wave flux being completely absorbed in the stratosphere (leading to a strong SSW) or a quasi-simultaneous reflection of all planetary wave components (leading to a substantial strengthening of the vortex). The co-evolution of polar vortex strength and vertical wave fluxes (Figure 3) is also consistent with quasi-linear interaction between the mean flow and vertically propagating waves 1 and 2, respectively, as follows. Prolonged upward wave 1 flux during late January weakened the polar vortex, effectively providing a pre-conditioning for subsequent wave 2 flux reaching deeper into the stratosphere around February 1st.

Ensembles initialized during the post-SSD period (ca. January 30th) produce comparatively accurate ensemble mean predictions for both the mid-February recovery of the polar vortex and the tropospheric extreme event around February 9th (Figures 1 and 9). In contrast, pre-SSD and SSD-onset ensembles only capture these events probabilistically (e.g., Figures 5 and 9). Pre-SSD ensemble members that do not experience a weak vortex period in February have generally increased values in $\tilde{AO}$ around February 9th (Figure 8). The timing of events and deterministic/probabilistic model behavior suggests a stratospheric wave-driven contribution to the formation of the corresponding tropospheric extreme event during/following the WRE (as also suggested by Lawrence et al., 2020). However, Figure 11 does not show any significant differences in tropospheric zonal mean zonal flow in early February. Tropospheric zonal mean anomalies only develop after the stratospheric flow anomalies, suggesting a persistent downward coupling of the zonal mean flows due to a strengthened polar vortex (e.g., Figure 6) rather than a rapid and direct downward coupling of the strat-trop flow during the WRE itself. In addition to zonal mean metrics, we also studied the direct response of the planetary wave components of the tropospheric geopotential height field (not shown), but could not identify a robust downward influence of the WRE.
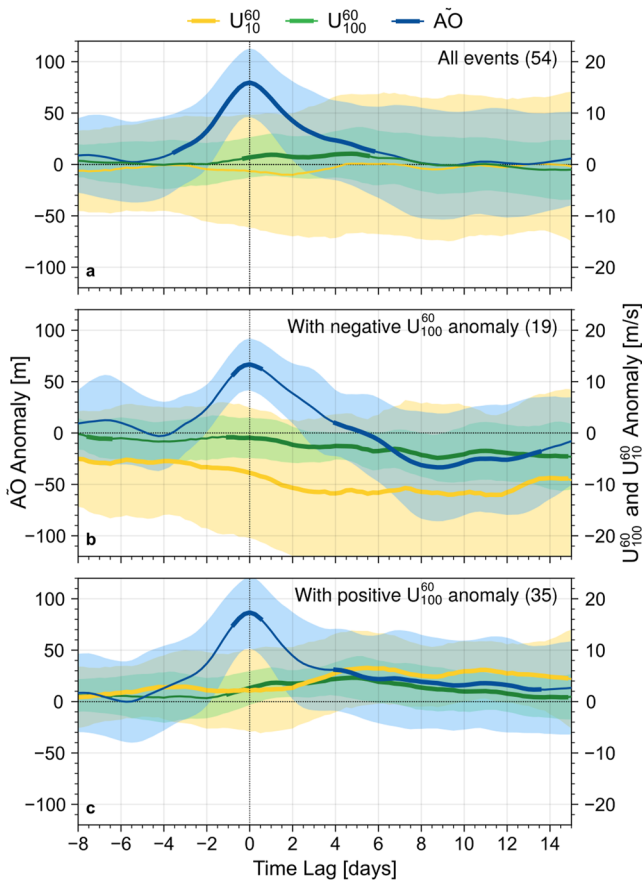
Figure 13. Composite evolution of $\tilde{AO}$, U_{100}^{60} and U_{10}^{60} anomalies for 54 extreme $\tilde{AO}$ events in a lagged ensemble initialized on February 18th and 21st. Events are defined as global maximum in $\tilde{AO}$ anomaly between March 9th and 23rd under the condition that $\tilde{AO} \geq 120m$ at the event date. Panel a shows all 54 events, while panels b and c show the events separated into two complementary clusters (19 and 35 members) that either have a positive or a negative U_{100}^{60} anomaly (when averaged over the 10 days following the event). The thick line-segments in panel a indicate periods where the composite mean of a respective index-anomaly is significantly different from zero, and in panels b and c periods with significant difference between the two cluster means (to 95% confidence in all cases). Shaded regions indicate composite variability in terms of one standard deviation.

The systematic correlation in predicted behavior between troposphere and stratosphere suggests a coupling between the two layers. In particular, the low predictability of the strong stratospheric winds in mid February suggests an influence of the troposphere via wave forcing (e.g., Figure 5 or 9). On the other hand, the persistently strong polar vortex in February and March increased the likelihood of anomalous tropospheric large-scale circulation as observed around February 21st. However, the strength and robustness of the corresponding downward influence of positive stratospheric circulation anomalies apparently depend on the strength of the anomaly and perhaps other factors. Figure 11 and S3 in Supporting Information S1 indicate a significant difference in tropospheric circulation strength ($\tilde{AO}$ index) in late February and early March between model realizations with a strong or weak stratospheric circulation (initialization in mid and late January). These significant differences in $\tilde{AO}$ may be largely attributed to the robust downward coupling of negative stratospheric zonal flow anomalies following weak vortex periods (or in extreme cases SSWs; cf. Figure 10). Consistently, the downward influence of strengthened polar vortices appears less robust in these ensemble simulations.

The changes in stratospheric zonal mean circulation are apparently connected to regional surface temperature signals via the tropospheric zonal mean circulation (cf. Figure S4 in Supporting Information S1). The ensemble's members with a relatively strong polar vortex reproduce a warm anomaly over the Eurasian continent in late February. However, the individual members show a large variety of troposphere-stratosphere evolutions in spite of the consistent coupling between stratospheric circulation anomalies and tropospheric response.

The downward influence of polar vortex strength anomalies is more robust for negative than for positive values. As a hypothesis we argue that this is caused by asymmetries in wave-mean flow interaction between weak versus strong polar vortices due to their different effects on the vertical propagation of planetary waves. Following Charney and Drazin (1961), waves can only propagate vertically if the basic state zonal wind u satisfies the two inequalities $0 < u < U_c$, where generally U_c is a function of the potential vorticity gradient, the meridional and zonal wave numbers, and perhaps other state characteristics. Correspondingly, the easterlies ($u < 0$) formed during SSWs typically pose critical lines that migrate downward; the radiative restoration of these mean flow anomalies is slow, especially in the lowermost stratosphere, providing long-lasting potential for downward coupling to the troposphere. On the other hand, strong vortex states do not exhibit such a clear threshold impacting wave propagation, except for extremely strong states such as those observed in SH mid-winter (Plumb, 1989). Even the strongest observed NH vortex states do not reach the typical mid-winter strength of the SH vortex.

The downward influence of the strengthened stratospheric polar vortex in late February and early March has potentially contributed to the anomalous tropospheric zonal circulation in late February and the persistently strengthened circulation in March (see Figure 1) and associated surface anomalies (Figure 2). As shown in Figure 13, the wind anomalies in the (lower) stratosphere can affect the likelihood, magnitude, and persistence of tropospheric circulation extremes (in terms of $\tilde{AO}$ anomaly). This downward influence should be regarded as a modification of probabilities (e.g., via modification of the tropospheric upper boundary condition) rather than a direct forcing of tropospheric anomalies as the tropospheric internal variability remains dominant. Table 1 shows that strong stratospheric flow anomalies generally strengthen positive tropospheric events, but weaken negative events (and vice versa for weak stratospheric winds). This can be interpreted as a shift in the probability distribution of tropospheric events toward more positive magnitudes and longer durations during periods with

Table 1
Different Properties of $\tilde{AO}$ Extreme Events Averaged Over 18 Ensembles (720 Members in Total) With Unevenly Spaced Initialization Dates Between January 10hr and March 12th

	All events	Positive U_{100}^{60} anomaly	Negative U_{100}^{60} anomaly
Positive $\tilde{AO}$ events			
Number of events	35	24	11
Persistence time [days]	2.6	4.3	1.9
Event magnitude [m]	80	86	65
Negative $\tilde{AO}$ events			
Number of events	36	15	21
Persistence time [days]	2.6	1.8	4.5
Event magnitude [m]	−76	−60	−87

Note. Events are defined via the time of local extreme $\tilde{AO}$ anomaly satisfying $\tilde{AO} \geq 100m$ (positive events) or $\tilde{AO} \leq 60m$ (negative events) any time between 15 and 38 days after initialization. Events have further been separated into two clusters with either positive or negative U_{100}^{60} ensemble anomaly (when averaged over the 10 days following the event). Shown are the number of events in the respective clusters, the cluster mean of *e*-folding decay time of the $\tilde{AO}$ anomaly for the events and the magnitude of the event in terms of $\tilde{AO}$ anomaly.

strengthened stratospheric winds. Similarly, the $\tilde{AO}$ probability distribution is shifted toward more negative anomalies during phases with weakened stratospheric winds and hence positive extreme events will tend to have a weaker magnitude and be less persistent. Thus, next to the interpretation of the downward influence of stratospheric flow anomalies as modification of probability distributions of the occurrence of specific tropospheric events, it can also be interpreted as a direct modification of the tropospheric event which is originally formed primarily due to internal tropospheric variability. Thus, if a positive tropospheric event happens to occur in a period with strengthened stratospheric winds, it will likely be modified due to downward coupling and thus be stronger in magnitude and more persistent. If, however, the same positive tropospheric event occurs during a phase with weakened stratospheric winds, it will generally be suppressed, leading to a weaker magnitude and a shorter event duration. Based on the current analyses, it is unclear if either of these interpretations is more adequate.

The sensitivity of tropospheric extremes on the general stratospheric state underlines the general robustness of stratospheric-tropospheric coupling, but also its highly probabilistic nature (see also (Baldwin & Dunkerton, 2001; Nakagawa & Yamazaki, 2006; E. Gerber et al., 2009)). Any changes in lower stratospheric winds can be interpreted as changes in flow restriction at the upper boundary of the purely tropospheric system, which then modify the corresponding internal flow evolution. The downward modification of tropospheric events by the lower stratospheric state is a rather robust process in early 2020, suggesting both the strong coupling of observed stratospheric and tropospheric extreme events and extreme persistence. However, it is not clear whether this coupling process was anomalously strong during the winter period of 2020 or if a similarly strong general downward influence can be observed in other years. This should be analyzed in further studies.

8. Summary and Conclusions

Eurasian weather in early 2020 was characterized by anomalously high temperatures and increased precipitation. These anomalous conditions were consistent with tropospheric wind anomalies and an associated shift in the mid-latitude jet (and corresponding Atlantic storm tracks). Further study of re-analysis data and numerical ensemble simulations suggest that the tropospheric extreme conditions were coupled to an extremely strong and zonally symmetric Northern hemispheric polar vortex in the stratosphere.

The substantial strengthening of the polar vortex in early February was mainly associated with a pronounced wave reflection event with persistently strong stratospheric winds for the following several weeks. This wave reflection event was particularly pronounced as it involved a quasi-simultaneous reflection of planetary waves with both zonal wave numbers 1 and 2. The event was preceded by a sudden stratospheric deceleration event, substantially decelerating upper stratospheric winds. The corresponding changes in the curvature of the zonal wind (and consistent changes in refractive index) created a vertically and meridionally confined wave guide in the extratropical stratosphere and thus ideal conditions for wave reflection. Our findings highlight that the vertical and meridional vortex structure plays an important role in determining whether upward wave fluxes get reflected or absorbed by the polar vortex. Due to this sensitivity and being the result of highly non-linear wave-mean flow interactions, WREs are difficult to predict. Therefore early February was a period of low stratospheric predictability, with predictions ranging from a strong recovery of the polar vortex to an increased likelihood of SSWs.

We presented evidence that the observed increase in polar vortex strength following the reflection event had an influence on the tropospheric flow and increased the likelihood of the formation of extreme values and the persistently positive phase of the $\tilde{AO}$ index in February and March (and the associated occurrence of extreme weather conditions in the troposphere). We further showed that during periods with a generally strong stratospheric polar vortex positive tropospheric $\tilde{AO}$ extreme events corresponding to a strengthened mid-latitude jet tend to occur more often and are generally stronger and more persistent, while negative events are suppressed. At the same time

positive $\tilde{AO}$ extremes in the troposphere couple upwards and strengthen the polar vortex, allowing for a mutual amplification of the two layers. A correspondingly equivalent mutual amplification can be found during periods with weakened stratospheric and tropospheric zonal mean jets. However, we find the downward influence of positive stratospheric zonal circulation anomalies to be overall less robust than the corresponding influence of negative anomalies.

Although the observed extreme circulation anomalies in the troposphere and stratosphere appear to be broadly connected, a detailed statistical analysis of large-ensemble simulations revealed a wide range of possible troposphere-stratosphere evolutions. This emphasizes the fortuitous nature of such rare circulation anomalies as observed during early 2020. Our results emphasize the generally robust dynamical coupling between stratosphere and troposphere in both directions, which for individual events nevertheless involves a large range of possible outcomes.

Data Availability Statement

The ERA5 re-analysis dataset used in this study can be accessed via the ECMWF website (https://www.ecmwf.int/en/forecasts/datasets/reanalysis-datasets/era5, last accessed August 2021). Details on the numerical model used are provided in Section 2.1, including information on model version, relevant parametrizations, and initial conditions. Datasets including the U_{10}^{60} and $\tilde{AO}$ time series for numerical ensembles and re-analysis data are provided in a public repository (DOI: https://doi.org/10.5282/ubm.data.281). The data for the EOF-based AO index and details on its computation can be accessed via the website of the National Oceanic and Atmospheric Administration (NOAA) Climate Diagnostics Center (CDC) under https://www.cpc.ncep.noaa.gov/products/precip/CWlink/daily_ao_index/ao.shtml (last accessed December 2021).

References

Albers, J. R., & Birner, T. (2014). Vortex preconditioning due to planetary and gravity waves prior to sudden stratospheric warmings. *Journal of the Atmospheric Sciences*, *71*(11), 4028–4054. https://doi.org/10.1175/jas-d-14-0026.1

Andrews, D., Mahlman, J., & Sinclair, R. (1983). Eliassen-palm diagnostics of wave-mean flow interaction in the gfdl" skyhi" general circulation model. *Journal of the Atmospheric Sciences*, *40*(12), 2768–2784. https://doi.org/10.1175/1520-0469(1983)040<2768:etwatm>2.0.co;2

Baldwin, M. P., Ayarzagüena, B., Birner, T., Butchart, N., Butler, A. H., Charlton-Perez, A. J., et al. (2021). Sudden stratospheric warmings. *Reviews of Geophysics*, *59*(1), e2020RG000708.

Baldwin, M. P., & Dunkerton, T. J. (2001). Stratospheric harbingers of anomalous weather regimes. *Science*, *294*(5542), 581–584. https://doi.org/10.1126/science.1063315

Baldwin, M. P., Stephenson, D. B., Thompson, D. W., Dunkerton, T. J., Charlton, A. J., & O'Neill, A. (2003). Stratospheric memory and skill of extended-range weather forecasts. *Science*, *301*(5633), 636–640. https://doi.org/10.1126/science.1087143

Beerli, R., & Grams, C. M. (2019). Stratospheric modulation of the large-scale circulation in the atlantic–european region and its implications for surface weather events. *Quarterly Journal of the Royal Meteorological Society*, *145*(725), 3732–3750. https://doi.org/10.1002/qj.3653

Birner, T., & Albers, J. R. (2017). Sudden stratospheric warmings and anomalous upward wave activity flux. *Sola*, *13* (Special_Edition), 8–12. https://doi.org/10.2151/sola.13a-002

Branković, Č., Palmer, T., Molteni, F., Tibaldi, S., & Cubasch, U. (1990). Extended-range predictions with ecmwf models: Time-lagged ensemble forecasting. *Quarterly Journal of the Royal Meteorological Society*, *116*(494), 867–912.

Charlton-Perez, A. J., Ferranti, L., & Lee, R. W. (2018). The influence of the stratospheric state on north atlantic weather regimes. *Quarterly Journal of the Royal Meteorological Society*, *144*(713), 1140–1151.

Charney, J., & Drazin, P. (1961). Propagation of planetary scale waves from the lower atmosphere to the upper atmosphere. *Journal of Geophysical Research*, *66*, 83–109. https://doi.org/10.1029/jz066i001p00083

Dacre, H. F., & Pinto, J. G. (2020). Serial clustering of extratropical cyclones: A review of where, when and why it occurs. *npj Climate and Atmospheric Science*, *3*(1), 1–10. https://doi.org/10.1038/s41612-020-00152-9

Dalchér, A., Kalnay, E., & Hoffman, R. N. (1988). Medium range lagged average forecasts. *Monthly Weather Review*, *116*(2), 402–416. https://doi.org/10.1175/1520-0493(1988)116<0402:mrlaf>2.0.co;2

Domeisen, D. I. (2019). Estimating the frequency of sudden stratospheric warming events from surface observations of the north atlantic oscillation. *Journal of Geophysical Research: Atmospheres*, *124*(6), 3180–3194. https://doi.org/10.1029/2018jd030077

Domeisen, D. I., & Butler, A. H. (2020). Stratospheric drivers of extreme events at the earth's surface. *Communications Earth & Environment*, *1*(1), 1–8. https://doi.org/10.1038/s43247-020-00060-z

Domeisen, D. I., Butler, A. H., Charlton-Perez, A. J., Ayarzagüena, B., Baldwin, M. P., Dunn-Sigouin, E., et al. (2020). The role of the stratosphere in subseasonal to seasonal prediction: 2. Predictability arising from stratosphere-troposphere coupling. *Journal of Geophysical Research: Atmospheres*, *125*(2), e2019JD030923. https://doi.org/10.1029/2019jd030923

Dunn-Sigouin, E., & Shaw, T. A. (2015). Comparing and contrasting extreme stratospheric events, including their coupling to the tropospheric circulation. *Journal of Geophysical Research: Atmospheres*, *120*(4), 1374–1390. https://doi.org/10.1002/2014JD022116

Gerber, E., Orbe, C., & Polvani, L. M. (2009). Stratospheric influence on the tropospheric circulation revealed by idealized ensemble forecasts. *Geophysical Research Letters*, *36*(24). https://doi.org/10.1029/2009gl040913

Gerber, E. P., Polvani, L. M., & Ancukiewicz, D. (2008). Annular mode time scales in the intergovernmental panel on climate change fourth assessment report models. *Geophysical Research Letters*, *35*(22). https://doi.org/10.1029/2008gl035712

Hardiman, S. C., Dunstone, N. J., Scaife, A. A., Smith, D. M., Knight, J. R., Davies, P., & Greatbatch, R. J. (2020). Predictability of european winter 2019/20: Indian ocean dipole impacts on the nao. *Atmospheric Science Letters*, *21*(12), e1005. https://doi.org/10.1002/asl.1005

Harnik, N. (2009). Observed stratospheric downward reflection and its relation to upward pulses of wave activity. *Journal of Geophysical Research: Atmospheres*, *114*(D8). https://doi.org/10.1029/2008JD010493

Harnik, N., & Lindzen, R. S. (2001). The effect of reflecting surfaces on the 985 vertical structure and variability of stratospheric planetary waves. *Journal of the Atmospheric Sciences*, *58* (19), 2872–2894. https://doi.org/10.1175/1520-0469(2001)058<2872:TEORSO>2.0.CO;2

Hersbach, H., Bell, B., Berrisford, P., Hirahara, S., Horányi, A., Muñoz-Sabater, J., et al. (2020). The era5 global reanalysis. *Quarterly Journal of the Royal Meteorological Society*, *146*(730), 1999–2049.

Hitchcock, P., & Simpson, I. R. (2014). The downward influence of stratospheric sudden warmings. *Journal of the Atmospheric Sciences*, *71*(10), 3856–3876.

Hoffman, R. N., & Kalnay, E. (1983). Lagged average forecasting, an alternative to Monte Carlo forecasting. *Tellus A: Dynamic Meteorology and Oceanography*, *35*(2), 100–118.

Huang, J., Hitchcock, P., Maycock, A. C., McKenna, C. M., & Tian, W. (2021). Northern hemisphere cold air outbreaks are more likely to be severe during weak polar vortex conditions. *Communications Earth & Environment*, *2*(1), 1–11.

Huntingford, C., Marsh, T., Scaife, A. A., Kendon, E. J., Hannaford, J., Kay, A. L., et al. (2014). Potential influences on the United Kingdom's floods of winter 2013/14. *Nature Climate Change*, *4*(9), 769–777.

Karpechko, A. Y., Hitchcock, P., Peters, D. H., & Schneidereit, A. (2017). Predictability of downward propagation of major sudden stratospheric warmings. *Quarterly Journal of the Royal Meteorological Society*, *143*(704), 1459–1470.

Katsafados, P., Papadopoulos, A., Varlas, G., Papadopoulou, E., & Mavromatidis, E. (2014). Seasonal predictability of the 2010 Russian heat wave. *Natural Hazards and Earth System Sciences*, *14*(6), 1531–1542.

Kautz, L.-A., Polichtchouk, I., Birner, T., Garny, H., & Pinto, J. G. (2020). Enhanced extended-range predictability of the 2018 late-winter eurasian cold spell due to the stratosphere. *Quarterly Journal of the Royal Meteorological Society*, *146*(727), 1040–1055.

Kolstad, E. W., Breiteig, T., & Scaife, A. A. (2010). The association between stratospheric weak polar vortex events and cold air outbreaks in the northern hemisphere. *Quarterly Journal of the Royal Meteorological Society*, *136*(649), 886–893.

Lawrence, Z. D., Perlwitz, J., Butler, A. H., Manney, G. L., Newman, P. A., Lee, S. H., & Nash, E. R. (2020). The remarkably strong arctic stratospheric polar vortex of winter 2020: Links to record-breaking arctic oscillation and ozone loss. *Journal of Geophysical Research: Atmospheres*, *125*(22), e2020JD033271.

Lee, S. H., Lawrence, Z. D., Butler, A. H., & Karpechko, A. Y. (2020). Seasonal forecasts of the exceptional northern hemisphere winter of 2020. *Geophysical Research Letters*, *47*(21), e2020GL090328.

Limpasuvan, V., Hartmann, D. L., Thompson, D. W., Jeev, K., & Yung, Y. L. (2005). Stratosphere-troposphere evolution during polar vortex intensification. *Journal of Geophysical Research: Atmospheres*, *110*(D24), D24101.

Lott, F., & Miller, M. J. (1997). A new subgrid-scale orographic drag parametrization: Its formulation and testing. *Quarterly Journal of the Royal Meteorological Society*, *123*(537), 101–127.

Mailier, P. J., Stephenson, D. B., Ferro, C. A., & Hodges, K. I. (2006). Serial clustering of extratropical cyclones. *Monthly Weather Review*, *134*(8), 2224–2240.

Matsuno, T. (1971). A dynamical model of the stratospheric sudden warming. *Journal of the Atmospheric Sciences*, *28*(8), 1479–1494.

Matthews, T., Murphy, C., Wilby, R. L., & Harrigan, S. (2014). Stormiest winter on record for Ireland and UK. *Nature Climate Change*, *4*(9), 738–740.

Nakagawa, K. I., & Yamazaki, K. (2006). What kind of stratospheric sudden warming propagates to the troposphere? *Geophysical Research Letters*, *33*(4), L04801.

Noguchi, S., Mukougawa, H., Kuroda, Y., Mizuta, R., Yabu, S., & Yoshimura, H. (2016). Predictability of the stratospheric polar vortex breakdown: An ensemble reforecast experiment for the splitting event in January 2009. *Journal of Geophysical Research: Atmospheres*, *121*(7), 3388–3404.

Orr, A., Bechtold, P., Scinocca, J., Ern, M., & Janiskova, M. (2010). Improved middle atmosphere climate and forecasts in the ecmwf model through a nonorographic gravity wave drag parameterization. *Journal of Climate*, *23*(22), 5905–5926.

Perlwitz, J., & Graf, H.-F. (2001). Troposphere-stratosphere dynamic coupling under strong and weak polar vortex conditions. *Geophysical Research Letters*, *28*(2), 271–274.

Perlwitz, J., & Harnik, N. (2003). Observational evidence of a stratospheric in1052 fluence on the troposphere by planetary wave reflection. *Journal of Climate*, *1053 16* (18), 3011–3026. https://doi.org/10.1175/1520-0442(2003)016<3011:OEOASI>2.0.CO;2

Perlwitz, J., & Harnik, N. (2004). Downward coupling between the stratosphere and troposphere: The relative roles of wave and zonal mean processes. *Journal of Climate*, *17*(24), 4902–4909. https://doi.org/10.1175/JCLI-3247.1

Pinto, J. G., Zacharias, S., Fink, A. H., Leckebusch, G. C., & Ulbrich, U. (2009). Factors contributing to the development of extreme north atlantic cyclones and their relationship with the nao. *Climate Dynamics*, *32*(5), 711–737.

Plumb, R. A. (1989). On the seasonal cycle of stratospheric planetary waves. *Pure and Applied Geophysics*, *130*(2), 233–242.

Polvani, L. M., & Waugh, D. W. (2004). Upward wave activity flux as a precursor to extreme stratospheric events and subsequent anomalous surface weather regimes. *Journal of Climate*, *17*(18), 3548–3554.

Priestley, M. D., Pinto, J. G., Dacre, H. F., & Shaffrey, L. C. (2017). The role of cyclone clustering during the stormy winter of 2013/2014. *Weather*, *72*(7), 187–192.

Rao, J., Garfinkel, C. I., & White, I. P. (2020). Predicting the downward and surface influence of the february 2018 and january 2019 sudden stratospheric warming events in subseasonal to seasonal (s2s) models. *Journal of Geophysical Research: Atmospheres*, *125*(2), 1–17.

Runde, T., Dameris, M., Garny, H., & Kinnison, D. (2016). Classification of stratospheric extreme events according to their downward propagation to the troposphere. *Geophysical Research Letters*, *43*(12), 6665–6672.

Rupp, P., & Birner, T. (2021). Tropospheric eddy feedback to different stratospheric conditions in idealised baroclinic life cycles. *Weather and Climate Dynamics*, *2*(1), 111–128.

Scaife, A., Karpechko, A. Y., Baldwin, M., Brookshaw, A., Butler, A., Eade, R., et al. (2016). Seasonal winter forecasts and the stratosphere. *Atmospheric Science Letters*, *17*(1), 51–56.

Shaw, T. A., & Perlwitz, J. (2013). The life cycle of northern hemisphere downward wave coupling between the stratosphere and troposphere. *Journal of Climate*, *26*(5), 1745–1763.

Shaw, T. A., Perlwitz, J., & Harnik, N. (2010). Downward wave coupling between the stratosphere and troposphere: The importance of meridional wave guiding and comparison with zonal-mean coupling. *Journal of Climate*, *23*(23), 6365–6381.

Sigmond, M., Scinocca, J., Kharin, V., & Shepherd, T. (2013). Enhanced seasonal forecast skill following stratospheric sudden warmings. *Nature Geoscience*, *6*(2), 98–102.

Taguchi, M. (2008). Is there a statistical connection between stratospheric sudden warming and tropospheric blocking events? *Journal of the Atmospheric Sciences*, *65*(4), 1442–1454.

Thompson, D. W., Baldwin, M. P., & Wallace, J. M. (2002). Stratospheric connection to northern hemisphere wintertime weather: Implications for prediction. *Journal of Climate*, *15*(12), 1421–1428.

Thompson, D. W., & Wallace, J. M. (1998). The arctic oscillation signature in the wintertime geopotential height and temperature fields. *Geophysical Research Letters*, *25*(9), 1297–1300.

Tomassini, L., Gerber, E. P., Baldwin, M. P., Bunzel, F., & Giorgetta, M. (2012). The role of stratosphere-troposphere coupling in the occurrence of extreme winter cold spells over northern europe. *Journal of Advances in Modeling Earth Systems*, *4*(4), M00A03.

Tripathi, O. P., Charlton-Perez, A., Sigmond, M., & Vitart, F. (2015). Enhanced long-range forecast skill in boreal winter following stratospheric strong vortex conditions. *Environmental Research Letters*, *10*(10), 104007.

Vogel, H., Förstner, J., Vogel, B., Hanisch, T., Mühr, B., Schättler, U., & Schad, T. (2014). Time-lagged ensemble simulations of the dispersion of the eyjafjallajökull plume over europe with cosmo-art. *Atmospheric Chemistry and Physics*, *14*(15), 7837–7845.

Wittman, M. A., Charlton, A. J., & Polvani, L. M. (2007). The effect of lower stratospheric shear on baroclinic instability. *Journal of the Atmospheric Sciences*, *64*(2), 479–496.

Woollings, T., Charlton-Perez, A., Ineson, S., Marshall, A., & Masato, G. (2010). Associations between stratospheric variability and tropospheric blocking. *Journal of Geophysical Research: Atmospheres*, *115*(D6), D06108.

Zängl, G., Reinert, D., Rípodas, P., & Baldauf, M. (2015). The icon (icosahedral non-hydrostatic) modelling framework of dwd and mpi-m: Description of the non-hydrostatic dynamical core. *Quarterly Journal of the Royal Meteorological Society*, *141*(687), 563–579.